Coupling of Protein Motion to Electron Transfer in a Photosynthetic Reaction Center: Investigating the Low Temperature Behavior in the Framework of the Spin–Boson Model

Dong Xu and Klaus Schulten*

August 23, 2000

*Department of Physics and Beckman Institute, University of Illinois at Urbana–Champaign, Urbana, IL 61801, USA

The spin–boson model is applied to describe the coupling between protein motion and electron transfer for the primary electron transfer in the photosynthetic reaction center of Rps. viridis, a coupling which involves a very large number of degrees of freedom of the protein. For this purpose the relationship between the spectral function $J(\omega)$ characterizing the protein motion and the fluctuations of the protein contribution to the energy gap is derived. The relationship allows one to determine a suitable $J(\omega)$ from classical Molecular Dynamics simulations. Furthermore, we provide also an efficient numerical method to determine electron transfer rates in the framework of the spin–boson model. We also derive a high temperature approximation for the transfer rate which connects the spin–boson description with the well-known descriptions by Marcus and Hopfield. We determine then electron transfer rates both as a function of the redox energy difference and of temperature. The results show that for the system considered, the Marcus theory holds well at physiological temperatures. The low temperature behavior of the electron transfer rates is in qualitative agreement with observations in that electron transfer can accelerate with lowering the temperature, and that transfer rates can also slightly decrease with decreasing temperature.

1 Introduction

One of the most essential questions regarding our understanding of protein functions is in how far the protein system needs to be described quantum mechanically. In general one assumes that the Born–Oppenheimer approximation can be applied and that electronic degrees are non-degenerate such that only a single electronic ground state contributes. One can then assume this state to be fixed and the nuclear degrees of freedom to move in a potential energy landscape defined through this ground state. In electron transfer systems the situation arises that two nearly degenerate electronic states exist, the state before and the state after the transfer and, hence, the Born–Oppenheimer approximation breaks down. In the case of weak coupling, the system being initially in the reactant state leaks slowly into the product state, and the aim of a description is to describe the rate of leakage assuming that the motion is governed by the energy landscape defined through the reactant state. This limit appears to be realized in many biological redox systems. It is well-known that such systems provide an excellent probe not only for the behavior of the electronic degrees of freedom, but also for the nuclear degrees of freedom (for a review see [1]). The most ominous property in this respect is the temperature dependence of electron transfer rates which in many cases are temperature independent or even increase when temperature is lowered from physiological temperatures to temperatures of liquid helium. Such behavior is a signature for quantum mechanical effects and, in fact, has been interpreted accordingly [1, 2].

Previous interpretations have assumed that quantum mechanical behavior arises through a small number of nuclear degrees of freedom which are particularly strongly coupled to the electron transfer reaction. However, as the simulations in [3–5] revealed, the coupling involves essentially all nuclear degrees of freedom of the protein. The observed temperature behavior implies that all degrees of freedom need to be described quantum mechanically, at least those degrees of freedom for which holds $k_B T \leq \hbar\omega_\alpha$, where ω_α is the frequency connected with the respective nuclear motion. Actually, at physiological temperatures there are many degrees of freedom in proteins with frequencies high enough to make a quantum mechanical description advisable, and the electron transfer provides an ideal context in which the need for quantum mechanical descriptions of the nuclear motion of proteins can be explored.

Of course, it is presently impossible to describe the nuclear degrees of freedom of a protein entirely quantum mechanically. We will pursue in the following a different route to test the quantum

mechanical character of nuclear motion coupled to electron transfer: we use the classical simulations in [3] to derive a model for the protein nuclear motion, which can be described by time-dependent perturbation theory [1].

1.1 Rationalization of the Spin–Boson Model

We will, in fact, employ the spin–boson model to describe the coupling between the motion of the protein matrix and the electronic degrees of freedom. In this model the motion of the protein atoms is idealized as a set of independent linear oscillators. The electronic degrees of freedom are simplified as well in that only two states, one for the reactants and one for the products, are employed; intermediate states, e.g., those describing electron tunneling, are neglected. The two state electron transfer system is equivalent to a spin–$\frac{1}{2}$ system, the atomic motion is described by a set of independent bosons, hence, the name spin–boson model. Figure 1 provides a good illustration of the photosynthetic reaction center of *Rhodopseudomonas viridis* from the spin–boson perspective: the figure shows the protein atoms, rendered in grey, in which are embedded, the prosthetic groups, rendered in black, involved in electron transfer: hemes, chlorophylls, pheophytines (all three featuring tetrapyrol rings) and quinones. The model attempts to describe how the thermal oscillations of the protein atoms couple to the various transfer steps of an electron moving along the prosthetic groups.

Previous investigations of the coupling of electron transfer and protein thermal motions were based on classical descriptions (see [3] and references therein). Such descriptions, namely, molecular dynamics simulations, are the starting point for our present investigation. The descriptions, as born out of the present study, agree rather well with quantum mechanical descriptions at physiological temperature. Hence, essential model parameters, namely those determining the frequency distribution of the oscillators (bosons) and the coupling strength, can be abstracted from classical molecular dynamics simulations. The spin–boson model then allows one to carry the description to the realm of lower temperatures. This domain, though not essential from a biological point of view, appears to shed some light on the mechanism of protein–electron transfer coupling in that a very untypical temperature dependence is observed as pointed out above: electron transfer rates vary little with temperature, defying the Arrhenius behavior of most chemical reactions, actually in some instances rates even increase when temperature is lowered.

The present investigation is by no means the first which accounts for a role of quantum mechanical vibrations coupled to electron transfer. The key new aspect of our investigation is two-fold: first, we base all model parameters on molecular dynamics simulations; second, the spin–boson model allows one to account for a very large number of vibrations, actually the model assumes the limit of infinitely many vibrations, rather than a small number. We will see that the spin–boson model may not yield qualitatively different predictions than models involving a small number of vibrational modes coupled to the electron transfer, but it certainly makes the role of the medium surrounding an electron transfer reaction appear in a new light: essentially all medium motions are coupled significantly to the reaction. The reason is surprisingly simple and applies clearly to the case of a protein as a medium: the coupling between electron transfer and medium is due to the Coulomb interaction. This interaction, however, is long range and encompasses a very large volume. The coupling results then from small additive contributions of many motions rather than from a few dominant motions. This finding of the molecular dynamics simulations paves the way for the spin–boson model.

[1] A preliminary version of this work has been published in [6].

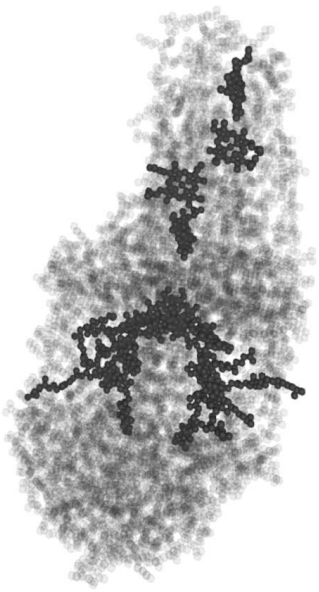

Figure 1: This figure shows the atoms of the photosynthetic reaction center (grey) and the prosthetic groups involved in the electron transfer (black). One can recognize in the upper part of the protein four heme groups. The center contains a sandwich complex of two chlorophylls from which stretch to both sides each a chlorophyll, a pheophytine and, towards the bottom, a quinone. These prosthetic groups conduct the electrons, the electron movement being accompanied by a response of the thermal motion of the (grey) protein atoms. The vibrations of these latter atoms are accounted for by the boson operators of the spin–boson model, individual transfer steps of the electron are described by a Hamiltonian expressed in terms of spin operators.

1.2 Hamiltonian of the Spin–Boson Model

A detailed review of the theory of the spin–boson model can be found in [7]. In the present setting of the coupling of electron transfer to medium thermal motions, the model describes the electronic degrees of freedom through a two–state Hamiltonian

$$\hat{H}_{el} \;=\; V\,\sigma_x \;+\; \frac{1}{2}\,\epsilon\,\sigma_z \tag{1}$$

where σ_x, σ_z are Pauli matrices, i.e., two elements of the three element basis of 2×2 Hermitian matrices. ϵ accounts for the energy difference of reactant and product states, and V accounts for the coupling between reactant and product states (the coupling originating from tunneling of the electron between electron donor and electron acceptor moieties). The medium thermal motion is described through an ensemble of independent linear oscillators with Hamiltonian

$$\hat{H}_{osc} \;=\; \sum_{\alpha} \left(\frac{\hat{p}_\alpha^2}{2\,m_\alpha} \;+\; \frac{1}{2}\,m_\alpha\,\omega_\alpha^2\,x_\alpha^2 \right) . \tag{2}$$

Here x_α denotes the spatial coordinate, $\hat{p}_\alpha$ the momentum operator of the oscillator, m_α its mass, and ω_α its frequency. The coupling between the vibrational degrees of freedom and the two–state system is linear in x_α and diagonal in the two-state system

$$\hat{H}_{coupl} \;=\; \frac{1}{2}\,q_0\,\sigma_z\;\sum_{\alpha} c_\alpha\,x_\alpha \tag{3}$$

where c_α describes the strength of the coupling of the electron transfer to the α-th oscillator and q_o is a constant scaling the overall coupling strength. The spin–boson Hamiltonian is the sum of all three contributions, i.e.,

$$\hat{H}_{sb} \;=\; \hat{H}_{el} \;+\; \hat{H}_{osc} \;+\; \hat{H}_{coupl}\;. \tag{4}$$

One may worry at this point that the many parameters which appear in the spin–boson model are impossible to specify uniquely and therefore, the model is either arbitrary or of limited use. However, the value of the spin–boson model, as advertised in [7], lies in the fact that only a certain average property of the system, the spectral function $J(\omega)$

$$J(\omega) \;=\; \frac{\pi}{2}\sum_{\alpha}\frac{c_\alpha^2}{m_\alpha\omega_\alpha}\,\delta(\,\omega\;-\;\omega_\alpha\,)\;, \tag{5}$$

and the energy difference ϵ and V need to be known. As long as one can assume that $J(\omega)$ is a smooth function determined by few parameters, there is ample opportunity to identify a proper $J(\omega)$. We elaborate below that the molecular dynamics simulations of the photosynthetic reaction center of *Rh. vir.* appear to be consistent with the choice of a simple spectral function. Hence, we claim that we have all the information to apply a proper spin–boson model to this protein system. In fact, the parameter V appears only in a factor V^2 which multiplies the electron transfer rate, the parentage of this functional form being the approximation involved in evaluating the electron transfer rate, namely, Fermi's golden rule. The energy difference ϵ will be left unspecified in the following; instead, we determine the rate as a function of ϵ following a procedure adopted in many previous investigations. One may then argue, for example, that in a biological electron transfer system ϵ has been selected such that the resulting electron transfer rate is near the maximum value.

1.3 Earlier Studies Based on the Spin–Boson Model

There exist various earlier studies which employed the spin–boson model for chemical reaction systems, in particular, for electron transfer systems. Onuchic et al. [8, 9] discussed the coupling of a bath of oscillators to a single nuclear reaction coordinate in the framework of the spin–boson model. The authors assumed a spectral function of the form

$$J_{eff}(\omega) \;=\; \frac{\eta\,\omega\,\Omega^4}{(\,\Omega^2\;-\;\omega^2\,)^2\;+\;4\,\gamma^2\,\omega^2} \tag{6}$$

which was adopted from a form of the spectral function employed by Caldeira and Leggett [7,10,11]

$$J_{eff}(\omega) \;=\; \eta\,\omega\exp\left(-\frac{\omega}{\Lambda}\right)\;. \tag{7}$$

Expanding the integrand in the Caldeira and Leggett formula as stated in equations (29, 30) below, the authors obtained results similar to those derived by means of the steepest descent method as presented in Sect. 3.1 of this paper. Onuchic [12] investigated also the case that the bath oscillators are coupled to a two-dimensional nuclear reaction coordinate employing a spectral function of the type

$$J_{eff}(\omega) \;=\; J^{y}_{eff}(\omega)\;+\;J^{z}_{eff}(\omega) \tag{8}$$

where $J^{y}_{eff}(\omega)$ and $J^{z}_{eff}(\omega)$ assume the analytical form (6) for two different sets of parameters η, Ω, γ, one representing coupling to slow outer sphere modes, e.g., solvent polarization, and the other representing coupling to a high frequency inner sphere vibrational mode. Onuchic represented also $J^{y}_{eff}(\omega)$ as a δ–function, a spectral function which by itself reduces in the underdamped limit the spin–boson model to the Hopfield model [2].

The models of Onuchic et al. [8,9,12] were not derived from simulations or experiments, rather, he and his co-authors investigated the spin–boson model in principle. The authors also did not state a practical way to determine suitable spectral densities from simulations or by other means.

Onuchic et al. assumed that one or two intramolecular modes of electron transfer are dominant. Rips and Jortner suggested that such kind of resonance effect is minor [13]. They applied a model Hamiltonian corresponding to two parabolic diabatic potential surfaces with adiabatic coupling between the surfaces. The authors derived a formula for the electron transfer rate, the same as (29) and (30) below, and they also determined the relationship between the time correlation function and spectral function [2] as stated in (77) below. Rips and Jortner employed the spectral function

$$J_{eff}(\omega) \;=\; \frac{\eta\,\omega}{1\;+\;\omega^2\,\tau^2}\;, \tag{9}$$

i.e., the same function which we adopt in the present investigation to account for the electron transfer rates. The authors then obtained an analytical expression for the electron transfer rate in terms of an infinity sum.

Mak and Chandler [14] also used the spectral function (9) to carry out Monte Carlo path integral simulations of electron transfer in organic liquids [14]. The authors matched the model to simulation results obtained for the energy–energy correlation function [15–17]. They demonstrated by means of simulations that at high temperature, the adiabatic free energy as a function of the energy gap, i.e., the potential energy difference felt by the electron at the different redox sites, is a nearly perfect parabola, a shape which is both consistent with the spin–boson model and with the classical Marcus theory of electron transfer [18, 19]. Such parabolic energy surface has also

[2] The $\epsilon^{''}(\omega)/|\epsilon(\omega)|^2$ used in [13] is the same as $J(\omega)$ in our case.

been obtained by other researchers from simulations [20, 21]. Chandler showed from the above results in [17] that the spin–boson model and the Marcus model are both essentially correct at high temperatures. Recently, Chandler and coworkers described a three-state spin–boson model in a photosynthetic reaction center and demonstrated the feature of an increase in the electron transfer rate with lowing of temperature for the case with essentially no activation energy between the initial state and the final state [22].

There exist also earlier studies which are compared to the present approach in Appendix C. Despite the similarity of the present investigations with all these earlier studies, there is still much difference. The authors of earlier studies did not carry out the systematical evaluation of electron transfer rates quantum mechanically as far as will be done below for the case of the photosynthetic reaction center where we provide the electron transfer rate as a function of the redox energy between reactant and product states as well as of temperature. Also, in our numerical calculation, we used a different approach from other authors', i.e., we did not apply any approximation to the spin-boson model itself, but rather solve the spin-boson model essentially exactly, however, choose an approximate spectral function for this purpose.

2 Quantum Mechanical Description of Coupling Between Medium and Electron Transfer

In this section, we introduce the spin-boson model [7] to describe the effect of the atomic motions of the protein matrix on the rate of the electron transfer $\mathrm{P}_S\mathrm{H}_L \rightarrow \mathrm{P}_S^+\mathrm{H}_L^-$ in the photosynthetic reaction center of *Rh. vir.* (for an introduction into this system see [3] and references cited therein). The spin–boson model assumes an ensemble of quantum oscillators linearly coupled to the electron transfer. The 2-state electron transfer system, the ensemble of quantum oscillators, and the coupling terms are collected in the spin–boson model Hamiltonian presented below in (15), which can be specified completely through observables determined in a classical molecular dynamics simulation like the one reported in [3].

2.1 Relationship Between Spin–Boson Hamiltonian and Protein Degrees of Freedom

As we have discussed above, the authors in [8, 9] have stated a spin-boson Hamiltonian which can account for electron transfer rates in proteins. In the following we would like to relate this Hamiltonian to a simple microscopic picture. The derivation allows one to interpret the parameters entering in the spin–boson Hamiltonian (1–4).

To illustrate the relationship of the spin–boson Hamiltonian to the microscopic coupling between electron transfer and medium we consider the well-known Marcus energy diagram presented in Fig. 2 [18, 19]. In this diagram, the free energy of both reactant and product states is described by a one–dimensional harmonic potential with identical force constants f. As shown in [3] this simple model accounts well for the simulated energy difference $\Delta E(t)$ between reactant and product electronic charge distributions: the diagram in Fig. 2 corresponds to a Gaussian distribution of energies $\Delta E(t)$, a distribution which is realized in molecular dynamics simulations [3, 4] and expected according to the central limit theorem [23]. $\Delta E(t)$ is here defined as follows: given a protein configuration defined through the positions of all M protein (medium) atoms $\vec{r}_1(t), \vec{r}_2(t), \ldots, \vec{r}_M(t)$ one evaluates the potential energy $V(\vec{r}_1, \vec{r}_2, \ldots \vec{r}_M)$ twice, once for an electronic charge distribution corresponding to the reactant state, i.e., $\mathrm{P}_S\mathrm{H}_L$, denoting the result by $E_R(t)$, and once for an electronic charge distribution corresponding to the product state, i.e., $\mathrm{P}_S^+\mathrm{H}_L^-$, denoting the result by $E_P(t)$; then it

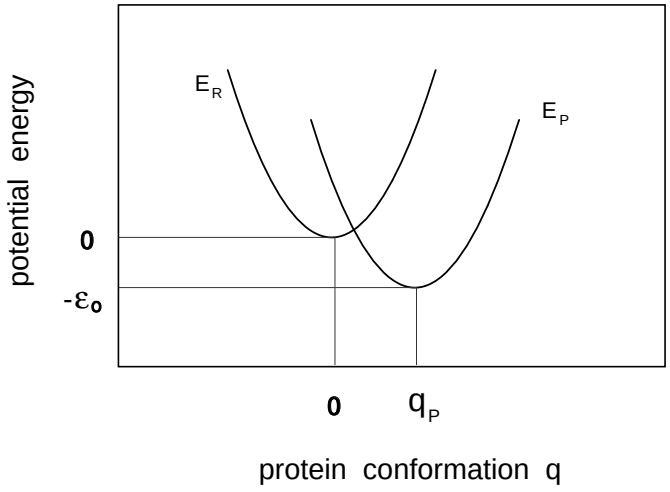

Figure 2: Sketch of potential energies before (E_R) and after (E_P) electron transfer as a function of a schematic conformational coordinate q. Indicated are the equilibrium position $q = 0$ and $q = q_P$ before and after electron transfer as well as the particular value of the redox energy difference ϵ_o corresponding to the presented potential energy curves.

holds that $\Delta E(t) = E_P(t) - E_R(t)$.

For the following description the reactant and product free energy curves are assumed to have the functional form

$$E_R = \frac{1}{2} f q^2 \tag{10}$$

and

$$E_P = \frac{1}{2} f (q - q_P)^2 - \epsilon_o . \tag{11}$$

In the above equations, q represents schematically the nuclear configuration of the protein matrix and q_P, ϵ_o represent the shift of the equilibrium position. As pointed out in [24] and [3], the potential functions presented in Fig. 2 are due to a dependence on thousands of nuclear coordinates, which define a many-dimensional potential-energy surface. q in Fig. 2 presents a parameter which really describes the Gaussian distribution of energy differences $\Delta E(t)$ as explained in [3]. The spin–boson model goes beyond the Marcus model as defined through Fig. 2 in that it allows one to represent a multitude of degrees of freedom coupled to the electron transfer through an ensemble of harmonic oscillators of various frequencies.

We will assume in the following that the nuclear degrees of freedom of the medium are too inert to change during the electron transfer step, i.e., we assume that the Born–Oppenheimer approximation can be applied and that the electron transfer is instantaneous with respect to the nuclear degrees of freedom. Let us assume that the protein matrix coupled to electron transfer can be represented through N different oscillators where N is of the order of magnitude of the number of atoms in the protein, i.e., about 10^4 in the case of the photosynthetic reaction center. We denote the frequencies of these oscillators by ω_α, $\alpha = 1, 2, \ldots, N$ and the associated vibrational coordinates by q_α, $\alpha = 1, 2, \ldots, N$. We assume that each mode is coupled to the electron transfer such that the harmonic potentials in the reactant state and in the product state differ as follows ($\alpha = 1, 2, \ldots, N$)

$$E_{R,\alpha} = \frac{1}{2} m_\alpha \omega_\alpha^2 q_\alpha^2 ,$$

$$E_{P,\alpha} \;=\; \frac{1}{2}\, m_\alpha\, \omega_\alpha^2\, (\, q_\alpha \,-\, q_{o,\alpha}\,)^2 \,-\, \epsilon_{o,\alpha}\;. \tag{12}$$

In this notation m_α are effective constants which do not need to be individually identified as we will see below.

The total energy in the reactant and product states is then

$$\begin{aligned} E_R &= \sum_{\alpha=1}^{N} \left(\frac{p_\alpha^2}{2m_\alpha} \,+\, \frac{1}{2}\, m_\alpha\, \omega_\alpha^2\, q_\alpha^2 \right)\;, \\ E_P &= \sum_{\alpha=1}^{N} \left(\frac{p_\alpha^2}{2m_\alpha} \,+\, \frac{1}{2}\, m_\alpha\, \omega_\alpha^2\, (\, q_\alpha \,-\, q_{o,\alpha}\,)^2 \,-\, \epsilon_{o,\alpha} \right)\;. \end{aligned} \tag{13}$$

The spin–boson Hamiltonian combines these energies with a quantum mechanical 2-state Hamiltonian as follows

$$\mathbf{H} \;=\; \begin{pmatrix} E_R & V \\ V & E_P \end{pmatrix}\;. \tag{14}$$

Using the expressions (13) and the Pauli spin matrices σ_j with $j = 1, 3$ one can obtain

$$\begin{aligned} \mathbf{H} \;=\;& V\,\sigma_1 \,+\, \frac{1}{2}\left(\sum_{\alpha=1}^{N} \epsilon_{o,\alpha} \right) \sigma_3 \,+\, \frac{1}{2}\left(\sum_{\alpha=1}^{N} m_\alpha \omega_\alpha^2 q_{o,\alpha}\, (q_\alpha \,-\, \frac{q_{o,\alpha}}{2}\,) \right) \sigma_3 \\ &+ \sum_{\alpha=1}^{N} \left(\frac{p_\alpha^2}{2m_\alpha} \,+\, \frac{1}{2}\, m_\alpha\, \omega_\alpha^2\, (\, q_\alpha \,-\, \frac{q_{o,\alpha}}{2}\,)^2 \right) \mathbb{1} \\ &+ \frac{1}{2} \sum_{\alpha=1}^{N} \left(\epsilon_{o,\alpha} \,+\, \frac{1}{4} m_\alpha \omega_\alpha^2 q_{o,\alpha}^2 \right) \mathbb{1}\;, \end{aligned} \tag{15}$$

which can be verified readily. The last term in (15) is proportional to the identical matrix $\mathbb{1}$, and thus can be omitted. Comparing (15) with the standard spin–boson Hamiltonian as given by (1–4) one can identify

$$\epsilon \;=\; \sum_{\alpha=1}^{N} \epsilon_{o,\alpha} \tag{16}$$

$$x_\alpha \;=\; q_\alpha \,-\, \frac{q_{o,\alpha}}{2} \tag{17}$$

$$q_o \;=\; 1 \tag{18}$$

$$c_\alpha \;=\; m_\alpha \omega_\alpha^2 q_{o,\alpha} \tag{19}$$

$$\begin{aligned} J(\omega) &= \frac{\pi}{2} \sum_{\alpha=1}^{N} \frac{c_\alpha^2}{m_\alpha \omega_\alpha}\, \delta(\omega \,-\, \omega_\alpha) \\ &= \frac{\pi}{2} \sum_{\alpha=1}^{N} m_\alpha \omega_\alpha^3 q_{o,\alpha}^2\, \delta(\omega \,-\, \omega_\alpha)\;. \end{aligned} \tag{20}$$

Actually, the derivation (14–20) has linked the multi-mode Marcus picture to an equivalent physical description, the spin–boson model. In this model the electron transfer is coupled linearly to an ensemble of independent oscillators which account for the protein motion, their equilibrium positions $q_{o,\alpha}/2$ in (17) being intermediate between the equilibrium positions $q_\alpha = 0$ before and $q_\alpha = q_{o,\alpha}$ after electron transfer as described in (12).

Having illustrated how the spin–boson Hamiltonian (1–4) is related to single harmonic degrees of freedom in the protein we will now proceed to specify a spin–boson Hamiltonian which is consistent with the simulations reported in [3].

2.2 Specification of the Spin–Boson Hamiltonian Consistent with a Classical Molecular Dynamics Simulation

Before embarking on the identification of a suitable Hamiltonian to describe the coupling between electron transfer and medium motions through a classical molecular dynamics simulation we like to point out that in the limit of high temperature classical and quantum descriptions should agree. As long as one can assume that the Hamiltonian is temperature independent, e.g., that the protein structure and hence the coupling terms do not change with temperature, one can expect that the classical simulations allow one to determine a suitable quantum mechanical model. The key parameters which determine how much the classical behavior applies at a particular temperature T are the ratios $\hbar\omega_\alpha/k_BT$ which should be small. Even though this ratio for the stiffest degrees of freedom does not assume small values at physiological temperatures, one finds that the majority of frequencies contributing to the medium–electron transfer coupling are small enough for the classical limit to be realized at $T = 300$ K, the highest temperature at which experiments and simulations are carried out. This statement will be borne out of the results of our calculations presented in Fig. 5a below. We will, therefore, start from the supposition that at the highest temperatures simulated quantum descriptions and classical descriptions coincide and that the classical simulations allow one to determine a suitable spin–boson model Hamiltonian.

We consider first the spectral function $J(\omega)$ which plays a prominent role in characterizing the spin–boson Hamiltonian. $J(\omega)$ should be represented by a smooth function that falls off at least as some negative power of ω for large ω [7]. In Appendix A it is shown that $J(\omega)$ is the Fourier–transform of the (normalized) energy–energy correlation function

$$C(t) \;=\; \frac{\langle\,(\,\Delta E(t)\;-\;\langle\Delta E\rangle\,)\,(\,\Delta E(0)\;-\;\langle\Delta E\rangle\,)\,\rangle}{\langle\,(\Delta E(0)\;-\;\langle\Delta E\rangle\,)\,(\,\Delta E(0)\;-\;\langle\Delta E\rangle\,)\,\rangle}\,, \tag{21}$$

an observable determined and discussed in the simulations of the photosynthetic reaction center of *Rhodopseudomonas viridis* reported in [3, 4].

In the simulations reported in [3], $C(t)$ exhibits an approximate exponential decay at high temperature. For the sake of simplicity we will assume that the energy–energy correlation function is well represented by a mono-exponential function.

By using equation (96) in Appendix A, one finds[3]

$$J(\omega) \;=\; \frac{\sigma^2\,\omega}{k_B\,T}\int_0^\infty dt\,e^{-t/\tau}\cos\omega t \;=\; \frac{\eta\,\omega}{1\;+\;\omega^2\,\tau^2}\;;\quad \eta \;=\; \frac{\sigma^2\tau}{k_B\,T}\,. \tag{22}$$

This form of $J(\omega)$ is so-called Debye function, and has been used also in several studies mentioned above [13, 14].

In [3] the values of τ and σ obtained from the simulation of the photosynthetic reaction center *Rps. viridis* are the following:

$$\tau \;=\; 94 \text{ fs} \;\; \text{(at high temperature)}\,; \tag{23}$$

$$\sigma \;=\; 3.9 \text{ kcal/mol} \;\; (T \;=\; 300 \text{ K})\,. \tag{24}$$

Actually according to [3], τ does not change significantly from $T = 80$ K to $T = 300$ K. According to (22), we obtain:

$$\eta\,/\,h \;=\; 25.15 \tag{25}$$

[3] In [7], an unspecified smooth cut-off ω_c is assumed which corresponds to an extra factor for $J(\omega)$, i.e., $J(\omega) \rightarrow J(\omega)\exp(-\omega/\omega_c)$. This factor avoids divergence as long as $V/\hbar$, $\epsilon/\hbar$, $kT/\hbar << \omega_c$ holds for the remaining parameters V and ϵ as well as the temperature. In the discussion in Section 3.1 such smooth cut-off will be assumed.

where h is Planck's constant. We have now identified the spectral function $J(\omega)$. As shown in [7], knowledge of the spectral function and ϵ suffices to determine the electron transfer rate as a function of temperature, i.e., to determine $k(T)$. In the following we will treat ϵ as a variable parameter rather than as a constant and evaluate the transfer rate as a function of ϵ and of temperature, i.e., evaluate $k(\epsilon, T)$. The rationale for this has been discussed at length in [3] and in the papers on electron transfer theories cited therein. We may just remind the reader that ϵ is to be interpreted as the difference in redox energies between P_S and H_L, i.e., a property identical to the standard free energy of reaction ΔG_o employed in the Marcus model (see [25]). This energy can be modified experimentally by replacement of the chromophores participating in the electron transfer [26, 27].

2.3 Expression for the Electron Transfer Rate

To determine the electron transfer rate $k(\epsilon, T)$, we employ an expression provided in [7]. The forward transfer rate ($P_S H_L \rightarrow P_S^+ H_L^-$) is ([7], eqn. 3.35)

$$k_{for}(\epsilon, T) \;=\; 2\left(\frac{V}{\hbar}\right)^2 \int_0^\infty dt \exp\left[\frac{-i\epsilon t}{\hbar} \;+\; \frac{iQ_1(t)}{\pi\hbar}\right] \exp\left[-\frac{Q_2(t)}{\pi\hbar}\right] \;\;, \tag{26}$$

so that the backward transfer rate ($P_S^+ H_L^- \rightarrow P_S H_L$) is

$$\begin{aligned} k_{back}(\epsilon, T) &= k_{for}(-\epsilon, T) \\ &= 2\left(\frac{V}{\hbar}\right)^2 \int_0^\infty dt \exp\left[\frac{i\epsilon t}{\hbar} \;+\; \frac{iQ_1(t)}{\pi\hbar}\right] \exp\left[-\frac{Q_2(t)}{\pi\hbar}\right] \;\;. \end{aligned} \tag{27}$$

The total transfer rate, i.e. the value actually measured in experiments, is

$$k(\epsilon, T) \;=\; k_{for}(\epsilon, T) \;+\; k_{back}(\epsilon, T) \tag{28}$$

$$= \left(\frac{2V}{\hbar}\right)^2 \int_0^\infty dt \cos\left(\frac{\epsilon t}{\hbar}\right) \cos\left[\frac{Q_1(t)}{\pi\hbar}\right] \exp\left[-\frac{Q_2(t)}{\pi\hbar}\right] \;\;. \tag{29}$$

Evaluation of this expression requires first an evaluation of the time-dependent functions $Q_1(t)$ and $Q_2(t)$ which are defined in terms of integrals over $J(\omega)$ as follows ([7], eqn. 3.36)

$$\begin{aligned} Q_1(t) &= \int_0^\infty d\omega\, \omega^{-2}\, J(\omega) \sin\omega t \\ Q_2(t) &= 2\int_0^\infty d\omega\;\; \omega^{-2} \sin^2\left(\frac{\omega t}{2}\right) \coth\left(\frac{\beta\hbar\omega}{2}\right)\; J(\omega) \;\;. \end{aligned} \tag{30}$$

Using the expression (22) for $J(\omega)$ one obtains

$$Q_1(t) \;=\; \int_0^\infty d\omega\, \frac{\eta \sin\omega t}{\omega\,(\,1 \;+\; \omega^2\tau^2\,)} \;=\; \frac{\eta\pi}{2}\;\left[\,1 \;-\; \exp\left(-\frac{t}{\tau}\right)\right] \tag{31}$$

and

$$Q_2(t) \;=\; \int_0^\infty d\omega\, \frac{2\,\eta \sin^2\left(\frac{\omega t}{2}\right)\, \coth\left(\frac{\beta\hbar\omega}{2}\right)}{\omega\,(\,1 \;+\; \omega^2\tau^2\,)} \tag{32}$$

where $\beta = 1/kT$. The latter expression, to our knowledge, cannot be expressed analytically. The electron transfer rate is then

$$\begin{aligned} k(\epsilon, T) &= \left(\frac{2V}{\hbar}\right)^2 \int_0^\infty dt \cos\left(\frac{\epsilon t}{\hbar}\right) \cos\left[\frac{\eta}{2\hbar}\left(1 \;-\; e^{-t/\tau}\right)\right] \;\times \\ &\quad \times \exp\left[-\frac{2\eta}{\pi\hbar}\int_0^\infty d\omega\, \frac{\sin^2\left(\frac{\omega t}{2}\right)}{\omega\,(\,1 \;+\; \omega^2\tau^2\,)} \coth\left(\frac{\beta\hbar\omega}{2}\right)\right] \;\;. \end{aligned} \tag{33}$$

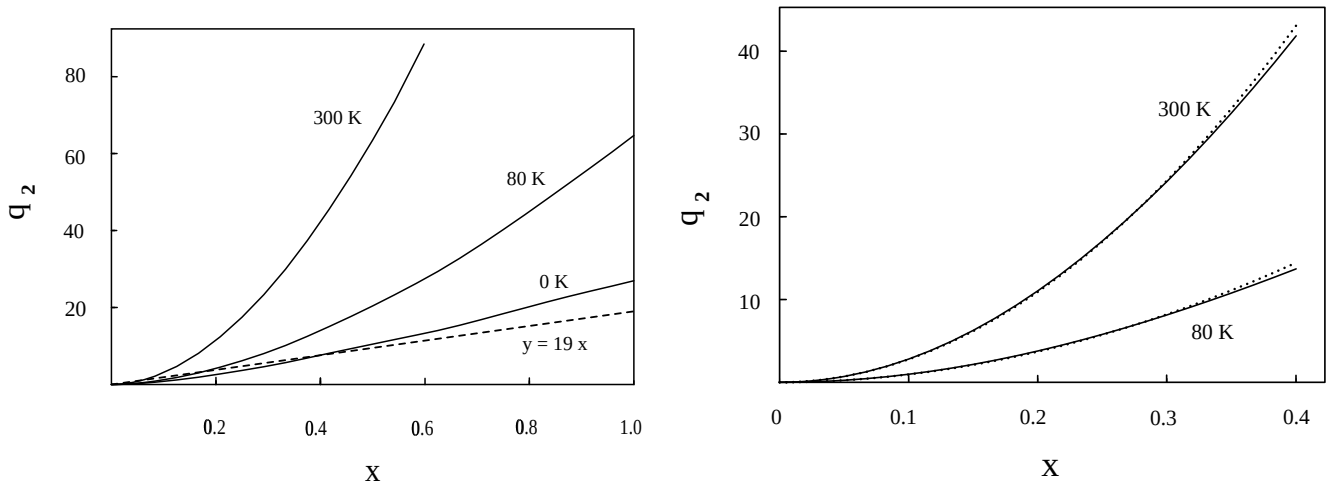

Figure 3: (a) Functional behavior of the quantity $q_2(x)$ as defined in (36) at three temperatures. The figure demonstrates that the $T = 0$ K curve is a lower bound for $q_2(x)$ and, that $y = 19x$ serves as a lower bound for all curves for $x > 0.4$. (b) Functional behavior of $q_2(x)$ defined in (36) in the interval [0, 0.4]. Shown are at two temperatures the exact values of $q_2(x)$ (————) and values resulting from the approximation (41) (· · · · · · · · ·).

In order to simplify this expression we define $x = t/\tau$, $y = \omega\tau$, and $\gamma = \eta/h$. This yields the final expression

$$\begin{aligned} k(\epsilon, T) &= \left(\frac{2V}{\hbar}\right)^2 \tau \int_0^\infty dx \cos\left(\frac{\epsilon\tau}{\hbar}\, x\right) \cos\left[\, \gamma\pi \, \left(1 - e^{-x}\right)\right] \times \\ &\quad \times \exp\left[-4\gamma \int_0^\infty dy \, \frac{\sin^2\left(\frac{xy}{2}\right)}{y\,(1 + y^2)} \coth\left(\frac{\hbar}{2k_B\tau} \cdot \frac{y}{T}\right)\right] . \end{aligned} \tag{34}$$

This expression contains three numerical constants which are specified according to the simulations in [3] as follows

$$\begin{aligned} \left(\frac{2V}{\hbar}\right)^2 \tau &= 9.40 \text{ ps}^{-1} \\ \frac{\tau}{\hbar} &= 6.20 \text{ mol/kcal} \\ \frac{\hbar}{2\,k_B\tau} &= 40.63 \text{ K}^{-1} . \end{aligned} \tag{35}$$

The stated numerical values result from $\tau = 94$ fs as determined in [3] and from $2V/\hbar = 10$ ps^{-1}. The latter value enters only as an overall scalar factor of the electron transfer rate, a property which is due to the Fermi golden rule approximation employed in [7] in deriving (29).

2.4 Numerical Evaluation of the Electron Transfer Rate

Equations (34, 35) allow one, in principle, to evaluate the electron transfer rate $k(\epsilon, T)$. However, straightforward numerical quadrature of (34) is very time consuming since it involves a double integral. We have carried out such calculation for a few ϵ and T values to establish the error involved in a numerical approximation. Such approximation will be derived now.

To achieve a faster, albeit approximate, evaluation of (34) we focus on the $\exp[\cdots]$ factor in the integrand of (34). We define

$$\begin{aligned} q_2(x) &= 4\gamma \int_0^\infty dy\, \frac{\sin^2\left(\frac{xy}{2}\right)}{y\,(1\,+\,y^2)} \coth\left(\frac{\hbar}{2k_B\tau}\cdot\frac{y}{T}\right) \\ &= 100.60 \int_0^\infty dy\, \frac{\sin^2\left(\frac{xy}{2}\right)}{y\,(1\,+\,y^2)} \coth\left(\frac{40.63\,y}{T}\right) \end{aligned} \tag{36}$$

where T is given in units of K. Figure 3a presents $q_2(x)$ for three different temperatures, $T = 0$, 80, 300 K. The calculations demonstrate that $q_2(x)$, at all three temperatures, is a monotonously increasing function of x, the increase being slowest for $T = 0$, i.e., $q_2(x)$ for $T = 0$ can be considered a lower bound for $q_2(x)$ at all other temperatures. The numerical calculations show, in particular, $q_2(x) > 19\,x$ for $x \geq 0.4$. This observation allows one then to estimate the contribution to $k(\epsilon, T)$ arising according to (34) from integration for $x \geq 0.4$. The following estimate results

$$\begin{aligned} &\left| 9.4 \int_{0.4}^\infty dx \cos(\,6.20\,\epsilon\,x\,)\,\cos[\,25.15\,\pi\,(1\,-\,e^{-x}\,)\,]\,\exp[\,-q_2(x)\,]\,\right| \\ &< \;9.4 \int_{0.4}^\infty dx \exp[\,-q_2(x)\,] \\ &< \;9.4 \int_{0.4}^\infty dx\, e^{-19x} \;\approx\; 4.7\,\times 10^{-3}\ \mathrm{ps}^{-1}\ . \end{aligned} \tag{37}$$

Obviously, the last value provides a very rough upper bound for the $\int_{0.4}^\infty dx\,\cdots$ contribution to $k(\epsilon, T)$, typical values of this contribution, in particular for higher temperatures, being much lower. Noting that from our calculations below result electron transfer rates in the range 1–0.1 ps^{-1} (c.f. Fig. 6a) the estimate (37) shows that the $\int_{0.4}^\infty dx\,\cdots$ contribution can be neglected and the electron transfer rate approximated as follows

$$k(\epsilon, T) \;=\; \frac{9.40}{\mathrm{ps}} \int_0^{0.4} dx \cos(\,6.20\,\epsilon\,x\,)\,\cos[\,25.15\,\pi\,(1\,-\,e^{-x})\,]\,\exp[\,-q_2(x)\,] \tag{38}$$

where ϵ is in units $kcal/mol$.

The functional form of $q_2(x)$ as shown in Fig. 3a reveals that this function assumes a minimum at $x = 0$. In fact, one can readily show

$$\left.\frac{dq_2}{dx}\right|_{x=0} \;=\; 0\ . \tag{39}$$

This suggests that one might approximate the x–integral in (34) through the steepest descent method expanding the exponential quadratically, i.e., using $q_2(x) \approx q_2(0) + q_2''(0)x^2$. Unfortunately, the second derivative $q_2''(0)$ diverges as can be seen from the expression

$$\left.\frac{d^2q_2(x)}{dx^2}\right|_{x=0} \;=\; 50.30 \int_0^\infty dy\, \frac{y\,\coth\left(\frac{40.63\,y}{T}\right)}{(1\,+\,y^2)} \;\rightarrow\; \infty\ . \tag{40}$$

However, one can approximate $q_2(x)$ rather well in the form

$$q_2(x) \;\approx\; q_2(0) \;+\; A\,x^\delta \tag{41}$$

with $1 < \delta < 2$ which also permits an efficient evaluation of $k(\epsilon, T)$[4].

[4]There is another way to simplify $q_2(x)$ into an approximate form analytically, see [6].

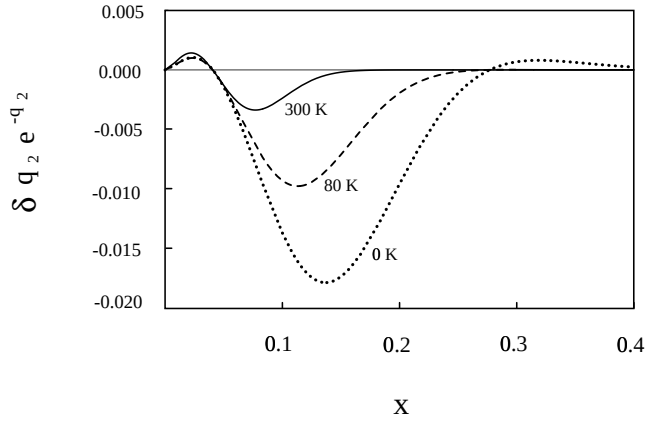

Figure 4: Functional behavior of the function $\delta q_2(x) \exp(-q_2(x))$ where $\delta q_2(x)$ is defined in (45). The function is shown at three temperatures to demonstrate that this function decreases with increasing temperature.

For the purpose of the numerical calculation we first note $q_2(0) = 0$ which follows from (36). To determine the constants A and δ in (41) we chose 100 points $x_j = 0.004\, j$, $j = 1, 2, \ldots, 100$ and evaluated through numerical quadrature of (37) $d_j = \ln q_2(x_j)$, $j = 1, 2, \ldots, 100$. Using a least square fit we matched the functional form $C + \delta \ln x$ to this series of points. The value C thus obtained yields A through $A = e^C$. The resulting δ is identical to the exponent in (41). The match between $q_2(x)$ evaluated by quadrature of (37) and (41) is presented in Fig. 3b. The comparison shows that (41) provides an excellent match to $q_2(x)$. The stated calculation revealed that A changes significantly with temperature whereas δ is insensitive to temperature, its value remaining close to 2 for all temperatures considered. Sample values of the parameters are at $T = 300$ K: $A = 264.381$, $\delta = 1.97963$; at $T = 80$ K: $A = 87.2766$, $\delta = 1.96274$; and at $T = 0$ K: $A = 47.2992$, $\delta = 1.93691$.

Since $q_2(x)$ is ϵ–independent one can use the same numerical approximation for all ϵ values considered. Hence, for a given temperature obtaining $k(\epsilon, T)$ at M different ϵ values requires one least square fit according to (41) and requires M simple numerical quadratures of [c.f. (38)]

$$k_{appr}(\epsilon, T) = \left(\frac{2V}{\hbar}\right)^2 \tau \int_0^\infty dx \cos\left(\frac{\epsilon\tau}{\hbar}\, x\right) \cos\left[\, \gamma\pi \, \left(1 - e^{-x}\right)\right] \, e^{-A(T)\, x^{\delta(T)}} \, . \tag{42}$$

Obviously, the numerical procedure chosen is much less time consuming than evaluating (34) by double quadrature.

2.5 Estimate of the Numerical Error in the Evaluation of Spin–Boson Transfer Rates

In the following we want to estimate the numerical error involved in the approximation adopted. We only account the error for fitting $q_2(x)$ here, but not for the errors of τ and σ^2. This error is defined as

$$\delta k(\epsilon, T) = k_{appr}(\epsilon, T) - k(\epsilon, T) \tag{43}$$

where $k_{appr}(\epsilon, T)$ is given by (42). Assuming that the error in $q_2(x)$ is small and confining the analysis to the integration interval $[0, 0.4]$ in which the dominant contribution arises (we estimated

already above the error due to neglecting the remaining integration interval) one obtains

$$\delta k(\epsilon,T) \;=\; \tfrac{9.40}{\rm ps}\int_0^{0.4} dx \cos\left(6.20\,\epsilon\,x\right)\,\cos[\,25.15\pi\,(1\,-\,e^{-x}\,]\,\times \\ \times\exp[\,-q_2(x)\,]\,\delta q_2(x) \tag{44}$$

where $q_2(x) \approx A\,x^{\delta}$ and

$$\delta q_2(x) \;=\; A\,x^{\delta}\;-\;q_2(x)\;. \tag{45}$$

Figure 4 presents the quantity $e^{-q_2(x)}\delta q_2(x)$ as a function of x for three different temperatures ($T\;=\;300, 80, 0$ K). One can recognize that the absolute value of this quantity is less than 0.02. We want to determine now the error arising from the integral in (45). For this purpose we note

$$\cos(6.20\epsilon x)\cos[\,25.15\pi\,(1\,-\,e^{-x})\,] \\ =\;\frac{1}{2}\,\{\,\cos[\,6.20\epsilon x\,+\,25.15\pi\,(1\,-\,e^{-x})\,]+\,\cos[\,6.20\epsilon x\,-\,25.15\pi\,(1\,-\,e^{-x})\,]\,\}\;. \tag{46}$$

The first term on the r.h.s. in (46) oscillates fast (at least ten oscillation periods in the interval $[0, 0.4]$) and, hence, it makes a negligible contribution to the integral in (45). An estimate of the numerical error in evaluating $k(\epsilon, T)$ is then given by

$$\begin{aligned}\delta k(\epsilon,T) \;&=\; \frac{4.7}{\rm ps}\int_0^{0.4} dx\cos[\,6.20\epsilon x\,-\,25.15\pi\,(1\,-\,e^{-x})\,]\,e^{-q_2(x)}\,\delta q_2(x) \\ &<\; \frac{4.7}{\rm ps}\int_0^{0.4} dx\;|\exp[\,-q_2(x)\,]\,\delta q_2(x)\,|\;.\end{aligned} \tag{47}$$

The bound provided is largest at $T\;=\;0$ K. In this worst case the bound is 0.01 ps^{-1}, the actual error being smaller, in particular, at higher temperatures. Since the rates evaluated below are mainly in the range 1—0.1 ps^{-1} (c.f. Figs. 5,6) one can conclude that the numerical procedure adopted provides accurate results.

3 High Temperature Approximation

In the following section we investigate the relationship between the electron transfer rate resulting from the spin–boson model and previous descriptions by Marcus and by Hopfield describing the bath motion coupled to electron transfer either classically or semiclassically. The relationship which can be derived in the high temperature limit allows one to interpret the characteristics of the spin–boson model, i.e., $J(\omega)$, in terms of the parameters appearing in the Marcus and Hopfield theories of electron transfer.

3.1 Steepest Descent Approximation for the Spin–Boson Transfer Rate

The expression (29) of the electron transfer rate together with the functional behavior of $Q_2(t)$ as shown in Fig. 3a suggests that one may employ the method of steepest descent, at least in the high temperature limit, for an approximate evaluation. This approximation is based on a quadratic expansion of $Q_2(t)$ around its minimum at $t\;=\;0$. The procedure requires one to determine the quantity

$$\mu \;=\; \frac{d^2}{dt^2}\,Q_2(t)\bigg|_{t=0}\;. \tag{48}$$

The expression for $Q_2(t)$ in (30) yields

$$\mu \;=\; \int_0^\infty d\omega J(\omega) \coth\left(\frac{\beta\hbar\omega}{2}\right) \;. \tag{49}$$

Unfortunately, for many choices of $J(\omega)$ this expression diverges and the steepest descent method cannot be applied. For this reason we chose to adopt the numerical scheme described in Section 2.4 involving the expansion $Q_2(t) \sim t^\delta$.

However, we note that the divergence of (49) is due to $\omega \to \infty$ contributions to the integral over $J(\omega)$. Since the number of modes in a protein are finite, the divergence in (49) is due to an artificial analytical form of $J(\omega)$. If one would assume a cut-off frequency ω_c, i.e., replace $J(\omega)$ by $J(\omega)\,\theta(\omega-\omega_c)$, or employ alternatively a smooth cut-off function (see footnote above), a divergence would not arise in (49). One may, hence, assume that the second derivative (48) actually exists, approximate

$$Q_2(t) \;\approx\; \frac{1}{2}\,\mu\, t^2 \;, \tag{50}$$

and employ this in a steepest descent method.

At a sufficiently high temperature, contributions to the integral in (29) arise only in a vicinity of $t = 0$ in which (50) is small. Assuming this vicinity to be narrow, i.e., μ as given in (49) to be large, one can approximate $Q_1(t)$ in (29) linearly around $t = 0$

$$Q_1(t) \;\approx\; \nu\, t\;; \quad \nu \;=\; \frac{d}{dt}\, Q_1(t)\Big|_{t=0} \;. \tag{51}$$

The expression for $Q_1(t)$ in (29) yields

$$\nu \;=\; \int_0^\infty d\omega\, \frac{J(\omega)}{\omega} \;. \tag{52}$$

Approximations (50) and (51) in (29) require one to evaluate

$$k(\epsilon,T) \;\approx\; \left(\frac{2V}{\hbar}\right)^2 \int_0^\infty dt \cos\left(\frac{\epsilon t}{\hbar}\right) \cos\left(\frac{\nu t}{\pi\hbar}\right) \exp\left(-\frac{\mu t^2}{2\pi\hbar}\right) \;. \tag{53}$$

The well-known formula

$$\int_0^\infty dx\, e^{-ax^2} \cos bx \;=\; \frac{1}{2}\sqrt{\frac{\pi}{a}} \exp\left(-\frac{b^2}{4a}\right) \tag{54}$$

leads to the expression

$$\begin{aligned} k(\epsilon,T) \quad &\approx\; \frac{2\pi V^2}{\hbar}\, \frac{1}{\sqrt{2\pi\delta^2}} \left\{ \exp\left[-\frac{(\epsilon\,-\,\epsilon_m)^2}{2\delta^2}\right] + \right. \\ &\qquad \left. \exp\left[-\frac{(\epsilon\,+\,\epsilon_m)^2}{2\delta^2}\right] \right\} \end{aligned} \tag{55}$$

$$\delta^2 \quad = \frac{\hbar\mu}{\pi} \;=\; \frac{\hbar}{\pi} \int_0^\infty d\omega\, J(\omega)\, coth\left(\frac{\beta\hbar\omega}{2}\right) \tag{56}$$

$$\epsilon_m \quad = \frac{\nu}{\pi} \;=\; \frac{1}{\pi} \int_0^\infty d\omega \frac{J(\omega)}{\omega} \;. \tag{57}$$

Comparing (26) (27) and (29) with (55)–(57), one can see that the first term in (55) correspondent to $k_{for}(\epsilon, T)$, and the second term $k_{back}(\epsilon, T)$ [5]. Approximation (55) becomes

$$k_{for}(\epsilon, T) \;\approx\; \frac{2\pi V^2}{\hbar}\,\frac{1}{\sqrt{2\pi\delta^2}}\exp\left[-\frac{(\epsilon\;-\;\epsilon_m)^2}{2\delta^2}\right]\;. \tag{58}$$

Equations (56–58) had been derived earlier by Garg et al. [8, 9].

According to (58) the maximum value of the electron transfer rate is

$$k_{for}^{(max)}(T) \;=\; k_{for}(\epsilon_m, T) \;=\; \frac{2\,\pi\,V^2}{\hbar}\,\frac{1}{\sqrt{2\,\pi\,\delta^2(T)}}\;. \tag{59}$$

From this follows immediately the relationship

$$\frac{k_{for}^{(max)}(T)}{k_{for}^{(max)}(0)} \;=\; \frac{\delta(0)}{\delta(T)} \;=\; \left[\frac{\int_0^\infty d\omega\, J(\omega)}{\int_0^\infty d\omega\, J(\omega)\coth\left(\frac{\beta\hbar\omega}{2}\right)}\right]^{\frac{1}{2}}\;. \tag{60}$$

This relationship can be compared with the corresponding expression for the Hopfield model

$$\frac{k_{for}^{(m,Hopf)}(T)}{k_{for}^{(m,Hopf)}(0)} \;=\; \left[\frac{\exp\left(\hbar\omega/k_BT\right)\;-\;1}{\exp\left(\hbar\omega/k_BT\right)\;+\;1}\right]^{\frac{1}{2}} \;=\; \sqrt{\tanh\left(\frac{\beta\hbar\omega}{2}\right)}\;. \tag{61}$$

One can readily verify that (60) and (61) are equivalent for $J(\omega)$ with a single frequency contribution, i.e., for $J(\omega) \sim \delta(\omega - \omega_o)$.

We like to point out again that according to the behavior shown in Fig. 3a the approximation involved in deriving (55–58) applies well at high temperatures. This can be concluded also from observing the property

$$\frac{\partial}{\partial T}Q_2(t,T) \;=\; \frac{\hbar}{2k_BT^2}\int_0^\infty d\omega\frac{J(\omega)}{\omega}\,(\,1\;-\;\cos\omega t\,)\,\mathrm{csh}^2\left(\frac{\beta\hbar\omega}{2}\right) \;>\; 0\;, \tag{62}$$

i.e., $Q_2(t, T)$ will be large enough at high temperatures such that the integral in (29) has contributions mainly for small t, such that (50, 51) hold well.

ϵ_m and δ^2 as given in (56, 57) can be expressed through the variance σ of the energy gap $\Delta E(t)$ defined in (97) (see Appendix A). Using (113) one can express

$$\epsilon_m \;=\; \frac{\sigma^2}{2k_BT}\;. \tag{63}$$

Assuming a cut-off frequency ω_c one determine that

$$\delta^2 \;=\; \frac{\hbar\mu}{\pi} \;=\; \frac{\hbar}{\pi}\int_0^{\omega_c} d\omega\, J(\omega)\, coth\left(\frac{\beta\hbar\omega}{2}\right)\;. \tag{64}$$

At a temperature high enough that $\hbar\omega_c/2k_BT << 1$ holds, one can approximate

$$\coth(\beta\hbar\omega/2) \;\approx\; 2/\beta\hbar\omega\;, \tag{65}$$

[5] As a matter of fact, when ϵ is large, one can neglect the contribution of $\exp[-(\epsilon+\epsilon_m)^2/2\delta^2]$ to $k(\epsilon, T)$ such that $k(\epsilon, T) \approx k_{for}(\epsilon, T)$.

which yields

$$\delta \;=\; \sigma \;. \tag{66}$$

According to the expression (58) one expects that $k(\epsilon, T)$ is a bell-shaped curve, at high temperatures a Gaussian, centered around ϵ_m as given in (63) and with a width σ. Since we assumed in our calculations that $J(\omega)$ for a protein is independent of temperature, according to (56), ϵ_m is temperature-independent and one expects that the position of the maximum of $k(\epsilon, T)$ is also largely independent of temperature. According to the expression (113) one can conclude that for temperature-independent $J(\omega)$ holds $\sigma \sim \sqrt{T}$ and, hence, the width of $k(\epsilon, T)$ should increase like $\sqrt{T}$ as well (c.f. Fig. 7 below). However, the zero point motion of quantum oscillators will prevent the width to vanish at low temperatures. Numerical calculations of the transfer rate according to expression (34, 35) employing the numerical approach described in Section 2.4 will show that the approximation (55–57), in the case of the photosynthetic reaction center, actually is accurate only for $T > 100$ K.

3.2 Comparison with Marcus Theory

The functional form of the electron transfer rate (58) agrees with the rate predicted by the classical Marcus theory of electron transfer if one identifies [c.f. (63, 66)]

$$\epsilon_m \;=\; \frac{\sigma^2}{2k_BT} \;=\; \frac{1}{2}\, f\, q_o^2 \tag{67}$$

$$\delta^2 \;\approx\; \sigma^2 \;=\; k_BT\, f q_o^2 \;. \tag{68}$$

The resulting functional form of the electron transfer rate is then

$$k_{for}^M(\epsilon, T) \;=\; \frac{2\,\pi\, V^2}{\hbar}\, \frac{1}{\sqrt{2\pi f k_BT q_o^2}} \exp\left[-\frac{(\epsilon \,-\, \frac{1}{2} f q_o^2)^2}{2k_BT f q_o^2} \right] \tag{69}$$

which in the Marcus theory of electron transfer corresponds to a single mode description of the bath. One may also interpret the parameters (67, 68) as being due to multi-mode representations of the medium in which case one would identify

$$\epsilon_m \;=\; \frac{\sigma^2}{2k_BT} \;=\; \sum_\alpha \frac{1}{2}\, m_\alpha \omega_\alpha^2\, q_{0,\alpha}^2 \tag{70}$$

$$\delta^2 \;\approx\; \sigma^2 \;=\; k_BT \sum_\alpha \frac{1}{2}\, m_\alpha \omega_\alpha^2\, q_{0,\alpha}^2 \;. \tag{71}$$

One can readily verify that this description is consistent with the description provided in Sect. 2.1 where we interpreted the spin–boson model in terms of an ensemble of linear oscillators. In particular, Eqs. (20, 57) are consistent with (70). One can, hence, state that the Marcus model and the spin–boson model both can be interpreted as describing the electron transfer being coupled to a bath of linear oscillators with reactant and product energies as described in (12), the difference lying in the (classical vs. quantum mechanical) treatment of the bath of oscillators.

It is also of interest to interpret the position ϵ_m of the maximum rate. According to (80) the average of the energy difference between reactant and product states, according to the derivation given in Appendix A, is

$$\langle \Delta E \rangle \;=\; -\,\epsilon \;+\; \epsilon_m \tag{72}$$

where ϵ_m is defined in (70). The maximum transfer rate occurs at $\langle \Delta E \rangle = 0$ (the average taken for the reactant state) which occurs for an ϵ–value at which the parabolas in Fig. 2 intersect at the minimum of the reactant potential $E_R(q)$.

3.3 Comparison with Hopfield Theory

The multi-mode Hopfield theory predicts a Gaussian form of the electron transfer rate like (58) with

$$\delta^2 \;=\; \frac{\hbar}{2}\sum_\alpha m_\alpha \omega_\alpha^3 q_{0\alpha}^2 \coth\left(\frac{\beta\hbar\omega_\alpha}{2}\right)\;. \tag{73}$$

One can readily relate this expression to the spectral function $J(\omega)$ using (20)

$$\delta^2 \;=\; \frac{\hbar}{\pi}\int_0^\infty d\omega\, J(\omega)\coth\left(\frac{\beta\hbar\omega}{2}\right)\;. \tag{74}$$

This expression is in agreement with (56). The agreement and the identity (70) imply that the high temperature limit (56, 57, 58) is, in fact, identical with the expression for the electron transfer rate as predicted by the Hopfield model.

The expression (74) can be employed only for spectral densities $J(\omega)$ for which the integral does converge, i.e., it cannot be employed for the spectral function (22). Since the divergence is due to contributions of artificially high frequencies one can introduce a cut-off frequency ω_c. A suitable choice is given by[6]

$$\hbar\,\omega_c \;=\; 3\,k_B\,T|_{T=300\ \mathrm{K}}\;. \tag{75}$$

The resulting numerical value for ω_c is 118 ps^{-1}. The simulation in [3] shows frequency distributions which have only small contributions for frequencies larger than this value. Also the thermal occupancy of higher vibrational excitations measured by $\exp(-\hbar\omega/k_BT)$ at $T = 300$ K is less than 5 percent for vibrations with frequencies higher than the chosen ω_c. Most important is the observation that the frequencies $\omega > \omega_c$ contribute only little to the correlation function $C(t)$ which served to obtain the spectral function $J(\omega)$ in the first place. In fact, using the expression (77) for $C(t)$ and the integration variable $y = \omega\,\tau$ one can express the change of $C(t)$ through this cut-off

$$\begin{aligned}\delta C(t) \;&\approx\; \frac{2}{\pi}\int_{11.08}^\infty dy\,\frac{\cos\left(yt/\tau\right)}{1\,+\,y^2} \\ &<\; \frac{2}{\pi}\int_{11.08}^\infty \frac{dy}{1\,+\,y^2} \;=\; \frac{2}{\pi}\left[-\arctan(11.08)\,+\,\frac{\pi}{2}\right] \;\approx\; 0.057\;.\end{aligned} \tag{76}$$

Since the initial decay of $C(t)$ for which a mono-exponential approximation can be assumed, involves numerical values in the range 1.0–0.1, the cut-off frequency implies only a minor alteration of the match of $C(t)$. We will, hence, assume the cut-off frequency ω_c as defined above when we use (73, 74) below, i.e., for the corresponding Hopfield approximation presented in Fig. 5b and Fig. 7.

4 Results

In this Section we discuss the electron transfer rates which result from a numerical evaluation of the expression (34, 35) employing the numerical approach described in Section 2.4 and for the Marcus and Hopfield models (58, 70, 71) and (58, 70, 74), respectively. In Fig. 5a we present electron transfer rates $k(\epsilon, T)$ as a function of the redox energy difference ϵ for temperatures $T = 0, 40, 80, 300$ K. $k(\epsilon, T)$ has a bell-shaped ϵ dependence, the shape being close to a Gaussian at high temperatures. This behavior is expected from the high temperature limit (56–58). The rate as a function of ϵ at low temperatures is asymmetrical. As expected from our discussion in Sect 3.1

[6]Since the integral in (74) has only a logarithmic divergence, the value of δ is not sensitive to the choice of ω_c.

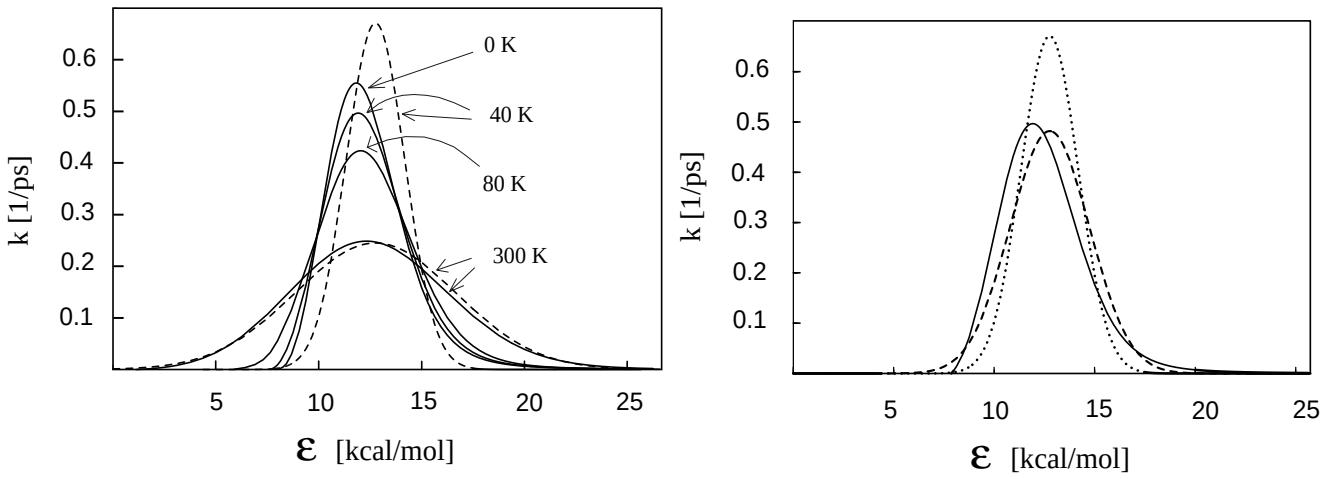

Figure 5: (a) Comparison of electron transfer rates $k(\epsilon, T)$ (————) shown as a function of ϵ at four different temperatures. The functions are centered approximately around ϵ_m as defined in (70). Presented are also rates resulting from the Marcus theory as defined through (58, 68, 70) (- - - - - -) at $T = 40, 300$ K. (b) Comparison of the rate $k(\epsilon, T)$ resulting from the spin–boson model (————), resulting from the Hopfield theory defined through (58, 70, 74) (- - - - - -), and resulting from the Marcus theory ($\cdots\cdots\cdots$) at $T = 40$ K.

the curves are also broader at high temperatures than at low temperatures and the position of the maximum of the functions $k(\epsilon, T)$ shift little from its high temperature position.

Figure 5a compares also the transfer rates predicted by the Marcus theory with those predicted by the spin–boson model. The rates $k(\epsilon, T)$ resulting for the Marcus theory agree well with those of the spin–boson model at $T = 300$ K, but differ significantly at $T = 40$ K. Figure 5b compares for $T = 40$ K the rates (34, 35) with the rates predicted by the Hopfield theory as discussed in Sect. 3.3 and with rates predicted by the Marcus theory. One observes that the Hopfield theory at this temperature provides a close match to the spin–boson rates and is significantly better than the rate of the Marcus theory.

The most important result in Fig. 5a is that at physiological temperatures the rates of the classical Marcus theory and of the quantum mechanical spin–boson model agree rather well. This outcome, of course, is very fortunate since it justifies at physiological temperatures a description of electron transfer in terms of models which describe the nuclear degrees of freedom classically. For example, the rates in Fig. 5a for $T = 300$, 80 K are very similar to those evaluated in [3] using an Ornstein-Uhlenbeck process to describe the coupling to the protein nuclear motion. However, Fig. 5a also reveals that at low temperatures very significant deviations from the classical Marcus theory develop: for the latter $k(\epsilon, T)$ becomes a δ–function for $T \to 0$, whereas the spin–boson model predicts a function with finite width; this function appears to be changing little between $T = 40$ K and $T = 0$ K.

The results in Fig. 5a,b agree with observations reported in [26] in that they show a distinct asymmetry with respect to ϵ_m at low temperatures. Such asymmetry is not predicted by the models of Marcus and Hopfield.

If one makes the assumption that biological electron transfer systems evolved their ϵ-values such that rates are optimized, one should expect that electron transfer rates in the photosynthetic reaction center are characterized through $\epsilon \approx \epsilon_m$. In Fig. 6a we present corresponding transfer rates $k(\epsilon, T)$ at ϵ values $\epsilon_m, \epsilon_m + \delta, \epsilon_m - \delta$ where $\delta = 2.5$ kcal/mol designates off-maximum positions.

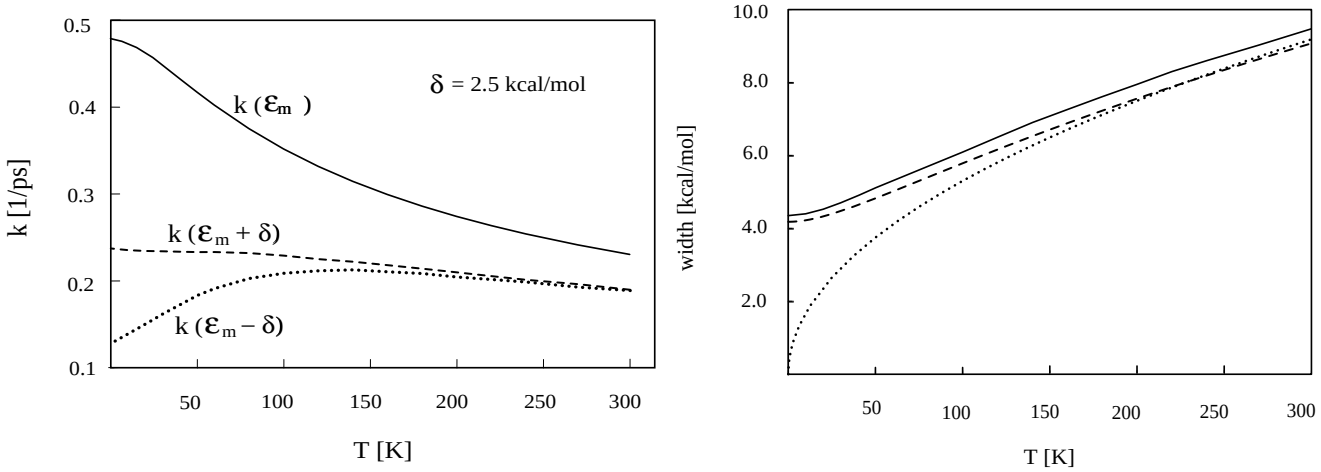

Figure 6: (a) Comparison of electron transfer rates $k(\epsilon_m, T)$, $k(\epsilon_m + \delta, T)$ and $k(\epsilon_m - \delta, T)$. $k(\epsilon_m, T)$ represents the fastest transfer rate of the system, the rates $k(\epsilon_m \pm \delta, T)$ are slower since their ϵ–values deviate from the optimal value ϵ_m. (b) Comparison of the temperature dependence of the width (as defined in the text) of the electron transfer rates $k(\epsilon)$. Shown are the widths of the rate corresponding to the spin boson model (————), the Hopfield theory (58, 70, 74) (- - - - - -), and the Marcus theory [(58, 68, 70)] (· · · · · · · · ·).

From experiments, the electron transfer processes in the photosynthetic reaction center show similar increases [28–32]. However, Fig. 6a demonstrates also that electron transfer at ϵ-values slightly off the maximum position can yield a different temperature dependence than that of $k(\epsilon_m, T)$, namely temperature independence or a slight decrease of the rate with decreasing temperature. Such temperature dependence has also been observed for biological electron transfer [32]. As Nagarajan et al. reported in [32] the temperature dependence of the transfer rate resembles that of $k(\epsilon_m, T)$ in photosynthetic reaction centers of native bacteria and in (M)Y210F mutants with tyrosine at the 210 position of the M–unit replaced by phenylalanine. However, a replacement of this tyrosine by isoleucine ((M)Y210I-mutant) yields a transfer rate which decreases like $k(\epsilon_m - \delta, T)$ shown in Fig. 6a. This altered temperature dependence should be attributed to a shift of the redox potentials, i.e., $\epsilon_m \rightarrow \epsilon_m - \delta$.

The width $\Delta\epsilon$ of the bell-shaped rate functions $k(\epsilon, T)$, defined through $k(\epsilon_m \pm \frac{1}{2}\Delta\epsilon, T) = \frac{1}{2}k(\epsilon_m, T)$, is presented in Figure 6b. The width increases at high temperatures approximately as $\sqrt{T}$ as expected in the framework of the Marcus theory. However, at low temperatures a dramatic deviation from the classical Marcus model can be observed in Fig. 6b: the width at about 100 K deviates from the $\sqrt{T}$ dependence and monotonously decreases with decreasing temperature towards a rather large value of about 4 kcal/mol at $T = 0$ K. Figure 6b demonstrates that this temperature dependence of the width is rather well represented by the Hopfield theory. It should be noted that a similar dependence of the width of the electron transfer rate has been reported in [31].

5 Summary

We have demonstrated that the spin–boson model is well suited to describe the coupling between protein motion and electron transfer in biological redox systems. The model accounts for the fact

that many protein degrees of freedom are coupled to redox processes. The model, through the spectral function $J(\omega)$ defined in (5), can be matched to the fluctuations of the protein contribution $\Delta E(t)$ to the redox energy differences through the relationships (21, 96) where $\Delta E(t)$ can be determined through a classical molecular dynamics simulation. We have demonstrated that the expressions for the electron transfer rates resulting for the spin–boson model can be evaluated numerically for a wide range of redox energy differences ϵ and temperatures T. In the high temperature limit the electron transfer rates for the spin–boson model match those of the well-known Marcus and Hopfield models, thereby establishing a straightforward interpretation of obtained transfer rates.

The main result regarding the electron transfer rates evaluated is that for a spectral function consistent with molecular dynamics simulations the spin–boson model at physiological temperatures predicts transfer rates in close agreement with those predicted by the Marcus theory. However, at temperatures below 100 K large deviations from the Marcus theory arise. The low temperature limit is discussed elsewhere [6]. The resulting low temperature rates are in qualitative agreement with observations, in particular, the spin–boson model explains the rise of transfer rates with decreasing temperature, and the asymmetric property of redox energy dependence.

The evaluation of the electron transfer rates in the framework of the spin–boson model has been based on second order perturbation theory and Fermi's golden rule. This approximation applies only as long as the function of vibrational states is high, a condition which is not satisfied at very low temperatures. It is desirable to extend the description to higher order perturbation theory or to other treatments. In this respect the calculation in [3] of electron transfer rates through the static ensemble approximation is of interest. The results reported in [3] demonstrate, however, that at physiological temperatures the deviation of a more exact treatment involving many orders of V from 2nd order perturbation theory, i.e., from the Marcus theory, is small. The theory above has also assumed that the spectral function $J(\omega)$ is temperature independent, an assumption which also deserves to be investigated. We have also described electron transfer in the adiabatic limit, in particular, we have not considered any coupling between protein degrees of freedom and the elementary event of electron tunneling.

The combination of simulation methods and analytical theory has proven to be a promising approach to investigate biological redox processes. Neither approach by itself can be successful since, on the one hand, proteins are too heterogeneous and ill understood to be molded into simple models, on the other hand, simulation methods are blind, leaving one with too much information and as a result, with none. The present example, connecting a single simulated observable, the medium redox energy contribution $\Delta E(t)$, with a model, the spin–boson model, which does not contain superfluous or undetermined parameters, most likely can be extended to other important protein reactions.

6 Acknowledgements

The authors like to thank A. Leggett for directing them towards the spin–boson model and for helpful advice. We are grateful to Mike Krogh for developing Figure 1 from our data. This work has been supported by the National Institute of Health (grant P41-RR05969). Computer time for this project has been made available by the National Center for Supercomputing Applications funded by the National Science Foundation.

Appendix A: Derivation of the Relationship Between $J(\omega)$ and $C(t)$

In the following we will derive the relationship which holds in the limit of high temperature between the spectral function $J(\omega)$ and the energy–energy correlation function $C(t)$, namely,

$$C(t) \;=\; \frac{\int_0^\infty d\omega\, \frac{J(\omega)}{\omega} \cos\omega t}{\int_0^\infty d\omega \frac{J(\omega)}{\omega)}} \;. \tag{77}$$

This relationship has been stated before in [13, 33] without detailed derivation. For the sake of completeness we provide the derivation here employing a different, simple approach.

We start from the definition of $C(t)$ in (21). Using

$$\Delta E \;=\; E_P \;-\; E_R \tag{78}$$

where E_R and E_P have been defined in (13) one obtains, introducing a time-dependence induced by the motion of the bath oscillators,

$$\Delta E(t) \;=\; -\sum_{\alpha=1}^{N} m_\alpha\, \omega_\alpha^2\, q_{o,\alpha}\, q_\alpha(t) \;+\; \sum_{\alpha=1}^{N} \left(\frac{1}{2}\, m_\alpha\, \omega_\alpha^2\, q_{o,\alpha}^2 \;-\; \epsilon_{o,\alpha} \right) \;. \tag{79}$$

The time average of $\Delta E(t)$ *before the electron transfer*, i.e., for $\langle q_\alpha \rangle = 0$, is

$$\langle \Delta E \rangle \;=\; \sum_{\alpha=1}^{N} \left(\frac{1}{2}\, m_\alpha\, \omega_\alpha^2\, q_{o,\alpha}^2 \;-\; \epsilon_{o,\alpha} \right) \;. \tag{80}$$

After the electron transfer holds $\langle q_\alpha \rangle = q_{o,\alpha}$ and, hence, the corresponding average of $\Delta E(t)$ is

$$\langle \Delta E \rangle_{\rm after} \;=\; -\sum_{\alpha=1}^{N} \left(\frac{1}{2}\, m_\alpha\, \omega_\alpha^2\, q_{o,\alpha}^2 \;+\; \epsilon_{o,\alpha} \right) \;. \tag{81}$$

One can write (80, 81)

$$\langle \Delta E \rangle \;=\; -\epsilon \;+\; \epsilon_m \;; \quad \langle \Delta E \rangle_{\rm after} \;=\; -\epsilon \;-\; \epsilon_m \tag{82}$$

where ϵ and ϵ_m are defined in (16) and in (67), respectively. The difference of the energy averages before and after electron transfer is

$$\langle \Delta E \rangle \;-\; \langle \Delta E \rangle_{\rm after} \;=\; 2\epsilon_m \;. \tag{83}$$

Using (80) the quantity $\delta E(t) = \Delta E - \langle \Delta E \rangle$ which enters the expression (21) for $C(t)$ is

$$\delta E(t) \;=\; -\sum_{\alpha=1}^{N} c_\alpha\, q_\alpha(t) \tag{84}$$

where

$$c_\alpha \;=\; m_\alpha\, \omega_\alpha^2\, q_{o,\alpha} \;. \tag{85}$$

q_α describes the motion of the bath oscillators with $\langle q_\alpha \rangle = 0$ before the electron transfer. In the high temperature limit the motion of all bath oscillators is classical and one has

$$q_\alpha(t) \;=\; A_\alpha \cos(\omega_\alpha t \;+\; \varphi_\alpha) \;. \tag{86}$$

The energy–energy correlation function (21)

$$C(t) \;=\; \frac{\langle \delta E(t)\, \delta E(0) \rangle}{\langle \delta E(0)\, \delta E(0) \rangle} \tag{87}$$

can then be written [we consider presently only the denominator $C_1(t)$ of (87)]

$$\begin{aligned} C_1(t) \quad &= \langle \delta E(t)\, \delta E(o) \rangle \\ &= \left\langle \left(\sum_{\alpha=1}^{N} c_\alpha\, A_\alpha \cos(\omega_\alpha t \,+\, \varphi_\alpha) \right) \left(\sum_{\alpha'=1}^{N} c_{\alpha'}\, A_{\alpha'} \cos\varphi_{\alpha'} \right) \right\rangle \\ &= \frac{1}{4} \langle \sum_{\alpha,\alpha'} c_\alpha\, c_{\alpha'}\, A_\alpha\, A_{\alpha'} \left[\exp\left(i\,(\omega_\alpha t \,+\, \varphi_\alpha \,+\, \varphi_{\alpha'}) \right) \,+ \right. \right. \\ &+ \exp\left(-i\,(\omega_\alpha t \,+\, \varphi_\alpha \,+\, \varphi_{\alpha'}) \right) \,+\, \exp\left(i\,(\omega_\alpha t \,+\, \varphi_\alpha \,-\, \varphi_{\alpha'}) \right) \,+ \\ &+ \left. \left. \exp\left(-i\,(\omega_\alpha t \,+\, \varphi_\alpha \,-\, \varphi_{\alpha'}) \right) \right] \rangle \end{aligned} \tag{88}$$

where φ_α and $\varphi_{\alpha'}$ are random numbers uniformly distributed in the interval $[0,\, 2\pi)$.

Carrying out the averages in (88) we follow the seminal derivation by Rayleigh [34, 35] and obtain

$$\langle \exp\left(i\,(\varphi_\alpha \,+\, \varphi_{\alpha'}) \right) \rangle \;=\; 0\,; \qquad \langle \exp\left(i\,(\varphi_\alpha \,-\, \varphi_{\alpha'}) \right) \rangle \;=\; \delta_{\alpha\alpha'}\,. \tag{89}$$

This yields

$$C_1(t) \;=\; \frac{1}{2} \sum_{\alpha=1}^{N} c_\alpha^2\, \langle\, A_\alpha^2 \,\rangle \cos\omega_\alpha t\,. \tag{90}$$

Using the well-known fact that the average energy of a harmonic oscillator is $k_B T$ one has

$$\frac{1}{2}\, m_\alpha\, \omega_\alpha^2\, \langle A_\alpha^2 \rangle \;=\; k_B\, T \tag{91}$$

and, hence,

$$C_1(t) \;=\; \sum_{\alpha=1}^{N} c_\alpha^2\, \frac{k_B T}{m_\alpha \omega_\alpha^2} \cos\omega_\alpha t \;\;. \tag{92}$$

The definition (20) of $J(\omega)$ yields finally

$$C_1(t) \;=\; \frac{2 k_B T}{\pi} \int_0^\infty \mathrm{d}\omega\, \frac{J(\omega)}{\omega} \cos\omega t\,. \tag{93}$$

Noting $C(t) \,=\, C_1(t)/C_1(0)$ one can conclude immediately (77).

We want to provide also an expression which allows one to determine $J(\omega)$ for a given correlation function $C(t)$. According to Fourier's theorem holds

$$\frac{2}{\pi} \int_0^\infty dt \cos\omega t \;\left[\int_0^\infty d\omega'\, \frac{J(\omega')}{\omega'} \cos\omega' t \;\right] \;=\; \frac{J(\omega)}{\omega} \tag{94}$$

and, hence,

$$\frac{J(\omega)}{\omega} \;=\; \frac{2}{\pi} \left[\int_0^\infty d\omega\, \frac{J(\omega)}{\omega} \right] \int_0^\infty dt\, C(t) \cos\omega t\,. \tag{95}$$

Using (113) in Appendix B we can conclude

$$\frac{J(\omega)}{\omega} \;=\; \frac{\sigma^2}{k_B\, T} \int_0^\infty dt\, C(t) \cos\omega t\,. \tag{96}$$

Accordingly, $J(\omega)$ can be determined from a molecular dynamics simulation recording the fluctuations of $\Delta E(t)$.

Appendix B: Relationship Between Spectral Density $J(\omega)$ and the Variance σ^2 of $\Delta E(t)$

The simulations reported in [3] show that $\Delta E(t)$ assumes a Gaussian distribution. Such distribution, except for the normalization, is described by a single parameter, the variance

$$\sigma^2 \;=\; \langle \Delta E^2 \rangle \;-\; \langle \Delta E \rangle^2 \; . \tag{97}$$

The spin–boson Hamiltonian assumes that the bath is an ensemble of linear oscillators characterized by a spectral function $J(\omega)$. In the following we want to demonstrate that the assumptions of the spin–boson model in the (classical) high temperature limit yields a Gaussian distribution of $\Delta E(t)$ as well and we will relate σ^2 and $J(\omega)$.

We will assume again that $\Delta E(t)$ is described through $\Delta E(t) \;=\; \delta E(t) \;+\; \langle \Delta E \rangle$ where $\delta E(t)$ is related through (84, 85) to the displacements of the bath oscillators before the electron transfer. Let us assume that there are N_α bath oscillators with the same frequency ω_α. We designate these oscillators by a second (beside α) index j. Then it holds, using (84–86),

$$\delta E(t) \;=\; \sum_\alpha \sum_j \, c_{\alpha j} \, A_{\alpha j} \cos\left(\omega_\alpha t \;+\; \varphi_{\alpha j}\right) \; . \tag{98}$$

We define

$$U_{\alpha j} \;=\; c_{\alpha j} \, A_{\alpha j} \cos\left(\omega_\alpha t \;+\; \varphi_{\alpha j}\right) \tag{99}$$

$$U_\alpha \;=\; \sum_j U_{\alpha j} \; . \tag{100}$$

The problem to solve the distribution of the quantities U_α as defined here has been solved by Rayleigh [34, 35]. Following his procedure one notes

$$\begin{aligned} U_\alpha \;&=\; \sum_{\alpha=1}^{N_\alpha} c_{\alpha j} \, A_{\alpha j} \cos\left(\omega_\alpha t \;+\; \varphi_{\alpha j}\right) \\ &=\; \cos\left(\omega_\alpha t\right) \sum_{\alpha=1}^{N_\alpha} c_{\alpha j} \, A_{\alpha j} \cos\varphi_{\alpha j} \;-\; \sin\left(\omega_\alpha t\right) \sum_{\alpha=1}^{N_\alpha} c_{\alpha j} \, A_{\alpha j} \sin\varphi_{\alpha j} \\ &=\; \gamma_\alpha \cos\left(\, \omega_\alpha t \;+\; \vartheta_\alpha \,\right) \end{aligned} \tag{101}$$

where

$$\gamma_\alpha \;=\; \sqrt{\left(\sum_{j=1}^{N\alpha} c_{\alpha j} A_{\alpha j} \cos\varphi_{\alpha j} \right)^2 \;+\; \left(\sum_{j=1}^{N\alpha} c_{\alpha j} A_{\alpha j} \sin\varphi_{\alpha j} \right)^2} \tag{102}$$

$$\tan\vartheta_\alpha \;=\; \left(\sum_{j=1}^{N\alpha} c_{\alpha j} A_{\alpha j} \sin\varphi_{\alpha j} \right) \Big/ \left(\sum_{j=1}^{N\alpha} c_{\alpha j} A_{\alpha j} \cos\varphi_{\alpha j} \right) \; . \tag{103}$$

Rayleigh has shown [35] that γ_α and ϑ_α are randomly distributed for large N_α. The distribution $p_\alpha(\gamma_\alpha)$ of γ_α is

$$p_\alpha(\gamma_\alpha) \;=\; \frac{2}{\delta_\alpha^2}\,\gamma_\alpha \exp\left(-\frac{\gamma_\alpha^2}{\delta_\alpha^2}\right)\;, \quad \delta_\alpha \;=\; \sum_{j=1}^{N_\alpha} c_{\alpha j}^2\, A_{\alpha j}^2\;. \tag{104}$$

The distribution of the phase angles ϑ_α is immaterial as the derivation below will show. According to the above calculations U_α behaves like a *single* oscillator with randomly distributed amplitudes γ_α and randomly distributed phases ϑ_α. Let us consider a particular oscillator of this ensemble described by fixed γ_α and ϑ_α

$$U_\alpha(t) \;=\; \gamma_\alpha \cos\left(\omega_\alpha t \,+\, \vartheta_\alpha\right)\;. \tag{105}$$

Sampling such $U_\alpha(t)$ at many time points $t \,=\, t_1, t_2, \ldots$ leads to a distribution [36]

$$\hat{p}_\alpha(U_\alpha) \;=\; \begin{cases} \frac{1}{\pi\sqrt{\gamma_\alpha^2 - U_\alpha^2}} & \text{for } U_\alpha \,\geq\, \gamma_\alpha \\ 0 & \text{for } U_\alpha \,<\, \gamma_\alpha\;. \end{cases} \tag{106}$$

We consider now again a large ensemble of oscillators (105) with a distribution of γ_α and ϑ_α values and ask for the probability that a particular U_α–value is realized. For the oscillator (105) all ensemble elements with $\gamma_\alpha \,\geq\, U_\alpha$ contribute. The distribution $\tilde{p}(U_\alpha)$ for the whole ensemble of bath oscillators is, therefore,

$$\begin{aligned} \tilde{p}(U_\alpha) \quad &=\; \int_{U_\alpha}^{\infty} d\gamma_\alpha\, p_\alpha(\gamma_\alpha)\, \hat{p}_\alpha(U_\alpha) \\ &=\; \int_{U_\alpha}^{\infty} d\gamma_\alpha\, \frac{2}{\delta_\alpha^2}\,\gamma_\alpha \exp\left(-\frac{\gamma_\alpha^2}{\delta_\alpha^2}\right)\, \frac{1}{\pi\,\sqrt{\gamma_\alpha^2 \,-\, U_\alpha^2}}\;. \end{aligned} \tag{107}$$

The integral can be expressed analytically. For this purpose we introduce the variable $y \,=\, \gamma_\alpha^2 - U_\alpha^2$. Using

$$\int_0^\infty dy\, \frac{1}{\sqrt{y}}\, e^{-\lambda y} \;=\; \sqrt{\frac{\pi}{\lambda}} \tag{108}$$

one obtains

$$\tilde{p}(U_\alpha) \;=\; \frac{1}{\sqrt{\pi\tilde{\sigma}^2}} \exp\left(-\frac{U_\alpha^2}{\tilde{\sigma}_\alpha^2}\right)\;, \tag{109}$$

i.e., a Gaussian distribution.

According to (98–100) holds $\delta E \,=\, \sum_\alpha U_\alpha$. Since each of the terms in this sum is Gaussian–distributed, the distribution of δE is a Gaussian as well, namely,

$$p(\delta E) \quad =\; \frac{1}{2\pi\sigma^2} \exp\left(-\frac{(\delta E)^2}{2\sigma^2}\right) \tag{110}$$

$$\sigma^2 \quad =\; \frac{1}{2}\sum_\alpha \sigma_\alpha^2 \;=\; \frac{1}{2}\sum_{\alpha,j} c_{\alpha j}^2\, A_{\alpha j}^2\;. \tag{111}$$

In the classical, i.e., high temperature, limit holds in equilibrium

$$\sigma^2 \;=\; \frac{1}{2}\sum_{\alpha,j} c_{\alpha j}^2\, \langle A_{\alpha j}^2 \rangle \;=\; \frac{1}{2}\sum_{\alpha,j} \frac{2\,k_B\,T}{m_{\alpha j}\,\omega_\alpha}^{\,2}\; c_{\alpha j}^2 \tag{112}$$

where we have used (91). We can then express, the sum over the coefficients $c_{\alpha j}^2$ through $J(\omega)$ using the definition of the latter,i.e., (5), and, hence, one can conclude

$$\sigma^2 \;=\; \frac{2k_BT}{\pi}\int_0^\infty d\omega\;\frac{J(\omega)}{\omega}\;. \tag{113}$$

Appendix C: Comparison with the Results of Other Researchers

Warshel et al. [37,38] developed the "dispersed polaron model" to calculate the electron transfer rate by simulation.

First, from a molecular dynamics simulation, they obtained the microscopic energy gap $\Delta E(t)$, which is actually the same as used in [3] and above. However, the authors evaluated the spectral function using a different approach, namely, Wiener-Khintchine theorem,

$$S\,(\omega) \;=\; \lim_{\tau\to\infty}\frac{|\,A\,(\omega,\tau)\,|^2}{2\tau} \tag{114}$$

$$\;=\; 2\int_0^\infty dt\,\cos\omega t\langle\,\Delta E(0)\,\Delta E(t)\,\rangle \tag{115}$$

where

$$A\,(\omega,\tau) \;=\; \int_{-\tau}^{\tau} dt\,\Delta E(t)\,e^{-i\omega t}\;. \tag{116}$$

From (89) and (90), one can easily show that $S(\omega)$ relates to the $J(\omega)$ in our case as follows

$$S\,(\omega) \;=\; \frac{2k_BTJ(\omega)}{\omega}\;. \tag{117}$$

Warshel et al. then calculated the forward electron transfer rate through Kubo's formula [39]:

$$k_{for} \;=\; \left(\frac{V}{\hbar}\right)^2\int_{-\infty}^{\infty} dt\,\exp\left[\,i\omega_{ba}\,t\;+\;\gamma(t)\,\right] \tag{118}$$

where V is the coupling constant described in (1),

$$\omega_{ba} \;=\; \frac{\langle\,\Delta E(t)\,\rangle}{\hbar}\;, \tag{119}$$

$$\gamma(t) \;=\; \frac{1}{\pi\hbar^2}\int_0^\infty d\omega(\,\cos\omega t\;-\;1\,)S\,(\omega)/\omega^2\;. \tag{120}$$

Warshel et al. [38] employed the model outlined to determine $S(\omega)$ numerically by (114) and (116), and then used $S(\omega)$ as an input to (120) to calculate the electron transfer rate. The authors also found that $C(t)$ exhibited a mono-exponential decay at $0 < t < 0.6\,\mathrm{ps}$, as described in [3, 4], but deviated from a mono-exponential at $0.6\,\mathrm{ps} < t < 1.3\,\mathrm{ps}$.

The above calculation gives certain quantum mechanical correction to the Marcus theory at low temperature. But as Bader et al. pointed out [33], the dispersed polaron method is a semiclassical approximation, which assume $[\,\hat{E}_R, \hat{E}_P\,] = 0$, where $\hat{E}_R$ and $\hat{E}_P$ are explained in (13) and (14), so

that it only gives good results in the classical limit i.e., at high temperatures, but overestimates the tunneling correction at low temperatures. As a matter of fact, one can show that Warshel et al.'s treatment is an approximation of the spin–boson model at high temperature. In fact, using (65), one can approximate $Q_2(t)$ in (32)

$$Q_2(t) \;\approx\; \int_0^\infty d\omega\, \omega^{-2}\,(1 \,-\, \cos\omega t)\,\frac{2}{\beta\hbar\omega}\,J(\omega)\;. \tag{121}$$

Comparing (117) (120) and (121), one obtains

$$\gamma(t) \;\approx\; \frac{Q_2(t)}{\pi\hbar}\;. \tag{122}$$

From (51) and (57) follows

$$Q_1(t) \;\approx\; \pi\epsilon_m t\;. \tag{123}$$

Considering (119), (82) and (123), one obtain

$$\omega_{ba} \;\approx\; \frac{\epsilon t}{\hbar} \,+\, \frac{Q_1(t)}{\pi\hbar}\;. \tag{124}$$

(122) and (124) implies that the dispersed polaron model expressed through the eqn (118) is an approximate high temperature form of the spin–boson model. Since $\coth(\beta\hbar\omega/2) > 2/\beta\hbar\omega$, $Q_2(t)$ is underestimated in (121), such that the electron transfer rate is overestimated in (118).

Following Warshel et al.'s work, Bader et al. developed an improved semiclassical approximation, namely the "the stationary phase approximation" [33] from a path integral expression. They determined $J(\omega)$ through the energy–energy correlation function $C(t)$ (21). These authors also adapted their choice of $J(\omega)$ to a simulation of electron transfer in liquids. In order to calculate the transfer rate for ferrous-ferric exchange in water, they used a spin–boson Hamiltonian as described through eqn. (1)-(4) except that they assumed $\epsilon = 0$. The electron transfer rate derived by these authors is [7]

$$\begin{aligned} k_{for} \;&=\; k_{back} \;=\; \frac{1}{2}\,k \\ &=\; \frac{2\pi V^2}{\hbar}\,\left[\,8\hbar\int_0^\infty d\omega J(\omega)\,\mathrm{cosech}(\beta\hbar\omega/2)\,\right]^{-1/2} \\ &\quad\times\exp\left[\,-\frac{4}{\pi\hbar}\int_0^\infty d\omega J(\omega)\,\omega^{-2}\tanh(\beta\hbar\omega/4)\,\right]\;. \end{aligned} \tag{125}$$

It is not easy to see the relation between (125) and (26) (27) for $\epsilon = 0$. But as Bader et al. claimed in [33], (125) agreed with the latter within 20% for $J(\omega)$ resulting from simulations.

[7] The notation [33] used is K, which is the same as V here, and $\Phi(\omega)$, which is equivalent to $2\,J(\omega)$.

References

[1] D. DeVault. *Quantum-Mechanical Tunneling in Biological Systems*. Cambridge University press, Cambridge, UK, 1984.

[2] J. J. Hopfield. Electron transfer between biological molecules by thermally activated tunneling. *Proc. Natl. Acad. Sci. USA*, 71:3640–3644, 1974.

[3] K. Schulten and M. Tesch. Coupling of bulk atomic motion to electron transfer: Molecular dynamics and stochastic quantum mechanics study of photosynthetic reaction centers. *Chemical Physics*, 158:421–446, 1991.

[4] M. Nonella and K. Schulten. Molecular dynamics simulation of electron transfer in proteins - theory and application to $Q_A \rightarrow Q_B$ transfer in the photosynthetic reaction center. *J. Phys. Chem.*, 95:2059–2067, 1990.

[5] Herbert Treutlein, Klaus Schulten, J.Deisenhofer, H.Michel, Axel Brünger, and Martin Karplus. Chromophore-protein interactions and the function of the photosynthetic reaction center: A molecular dynamics study. *Proc. Natl. Acad. Sci. USA*, 89:75–79, 1991.

[6] Dong Xu and Klaus Schulten. Multi-mode coupling of protein motion to electron transfer in the photosynthetic reaction center: Spin-boson theory based on a classical molecular dynamics simulation. In J. Breton and A. Vermeglio, editors, *The Photosynthetic Bacterial Reaction Center: II. Structure, Spectroscopy and Dynamics*, NATO ASI Series A: Life Sciences, pages 301–312. Plenum Press, New York, 1992.

[7] A. J. Leggett, S. Chakravarty, A. T. Dorsey, M. P. A. Fisher, A. Garg, and W. Zwerger. Dynamics of the dissipative two-state system. *Rev. Mod. Phys.*, 59:1–85, 1985.

[8] A. Garg, J. N. Onuchic, and V. Ambegaokar. Effect of friction on electron transfer in biomolecules. *J. Chem. Phys.*, 83:4491–4503, 1985.

[9] J. N. Onuchic, D. N. Beratan, and J. J. Hopfield. Some aspects of electron-transfer reaction dynamics. *J. Phys. Chem.*, 90:3707–3721, 1986.

[10] A. O. Cardeira and A. J. Leggett. Quantum tunnelling in a dissipative system. *J. Ann. Phys.(N.Y.)*, 149:374–456, 1983.

[11] A. O. Cardeira and A. J. Leggett. Path integral approach to quantum brownian motion. *Physica A*, 121:587–616, 1983.

[12] J. N. Onuchic. Effect of friction on electron transfer: The two reaction coordinate case. *J. Chem. Phys.*, 86:3925–3943, 1987.

[13] Ilya Rips and Joshua Jortner. Dynamic solvent effects on outer-sphere electron transfer. *J. Chem. Phys.*, 87:2090–2104, 1987.

[14] C. H. Mak and D. Chandler. Solving the sign problem in quantum monte carlo dynamics. *Phys. Rev. A*, 41:5709–5712, 1990.

[15] R. A. Kuharsky, J. S. Bader, D. Chandler, M. Sprik, M. L. Klein, and R. W. Impey. Molecular model for aqueous ferrous–ferric electron transfer. *J. Chem. Phys.*, 89:3248–3257, 1988.

[16] J. S. Bader and D. Chandler. Computer simulation of photochemically induced electron transfer. *Chem. Phys. Lett.*, 157:501–504, 1989.

[17] D. Chandler. Computer simulation of electron transfer. *chemica scripta*, 29A:61–62, 1989.

[18] R. A. Marcus. On the energy of oxidation-reduction reactions involving electron transfer. I. *J. Chem. Phys.*, 24:966–978, 1956.

[19] R. A. Marcus. Electrostatic free energy and other properties of states having nonequilibrium polarization. II. *J. Chem. Phys.*, 24:979–989, 1956.

[20] Jenn-Kang Hwang and Arieh Warshel. Microscopic examination of free-energy relationship for electron transfer in polar solvent. *J. Am. Chem. Soc.*, 109:715–720, 1987.

[21] Chong Zheng, J. Andrew McCammon, and Peter G. Wolynes. Quantum simulation of nuclear rearrangement in electron transfer reactions. *Proc. Natl. Acad. Sci. USA*, 86:6441–6444, 1989.

[22] M. Marchi, J. N. Gehlen, D. Chandler, and M. Newton. Diabatic surfaces and the pathway for primary electron transfer in a photosynthetic reaction center. *J. Am. Chem. Soc.*, 115(10):4178–4190, 1993.

[23] C. W. Gardiner. *Handbook of Stochastic Methods*. Springer, New York, 1983.

[24] R. A. Marcus and N. Sutin. Electron transfers in chemistry and biology. *Biochem. Biophys. Acta*, 811:265–322, 1985.

[25] H. Sumi and R. A. Marcus. Dynamical effects in electron transfer reactions. *J. Chem. Phys.*, 84:4894–4914, 1986.

[26] M. R. Gunner and P. Leslie Dutton. Temperature and ΔG_o dependence of the electron transfer from BPh^- to Q_a in a reaction center protein from *rhodobacter sphaeroides* with different quinones as Q_a. *J. Am. Chem. Soc.*, 111:3400–3412, 1989.

[27] C. Kirmaier, D. Gaul, R. DeBrey, D. Holten, and C. Schenk. Charge separation in a reaction center incorporating bacteriochlorophyll for photoactive bacteriopheophytin. *Science*, 251:922–927, 1991.

[28] G. Feher, T. R. Arno, and M. Y. Okamura. The effect of an electric field on the charge recombination rate of $D^+Q_A^- \rightarrow DQ_A$ in reaction centers from *rhodobacter sphaeroides* R-26. In J. Breton and A. Vermeglio, editors, *The Photosynthetic Bacterial Reaction Center: Structure and Dynamics*, pages 271–287, New York and London, 1988. Plenum Press.

[29] M. Bixon and J. Jortner. Coupling of protein modes to electron transfer in bacterial photosynthesis. *J. Phys. Chem.*, 90:3795–3800, 1986.

[30] J. L. Martin, J. Breton, J. C. Lambry, and G. Fleming. The primary electron transfer in photosynthetic purple bacteria: Long range electron transfer in the femtosecond domain at low temperature. In J. Breton and A. Vermeglio, editors, *The Photosynthetic Bacterial Reaction Center: Structure and Dynamics*, pages 195–203, New York and London, 1988. Plenum Press.

[31] C. Kirmaier and D. Holten. Temperature effects on the ground state absorption spectra and electron transfer kinetics of bacterial reaction centers. In J. Breton and A. Vermeglio, editors, *The Photosynthetic Bacterial Reaction Center: Structure and Dynamics*, pages 219–228, New York and London, 1988. Plenum Press.

[32] V. Nagarajan, W. W. Parson, D. Gaul, and C. Schenck. Effect of specific mutations of tyrosine-(m)210 on the primary photosynthetic electron-transfer process in rhodobacter sphaeroides. *Proc. Natl. Acad. Sci. USA*, 87:7888–7892, 1990.

[33] J. S. Bader, R. A. Kuharski, and D. Chandler. Role of nuclear tunneling in aqueous ferrous-ferric electron transfer. *J. Chem. Phys.*, 93:230–236, 1990.

[34] Lord Rayleigh. *The Theory of Sound, Vol. I, 2nd ed.* MacMillan and Company Ltd., London, 1894.

[35] Lord Rayleigh. *Scientific Papers, Vol. I, p491 and Vol. IV, p370.* Cambridge University Press, Cambridge, England, 1899–1920.

[36] V. K. Thankappan. *Quantum Mechanics.* John Wiley & sons, New York, 1985.

[37] Arieh Warshel and Jenn-Kang Hwang. Simulations of the dynamics of electron transfer reactions in polar solvent: Semiclassical trajectories and dispersed polaron approaches. *J. Chem. Phys.*, 84:4938–4957, 1986.

[38] A. Warshel, Z. T. Chu, and W. W. Parson. Dispersed polaron simulations of electron transfer in photosynthetic reaction center. *Science*, 246:112–116, 1989.

[39] R. Kubo and Y. Toyozawa. Application of the method of generating function to radiative and non-radiative transitions of a trapped electron in a crystal. *Prog. Theoret. Phys.*, 13:160–182, 1955.